Titles: Distinct Flower signaling domains orchestrate cellular fitness via secreted vesicles in Aβ-induced neurodegeneration

Szu-Min Tu[1,2], Ching-Hsin Lin[1,2], Yang Liu[2,3], Johannes Hohneck[4], Martin Jung[5], Annika Clemenz[6], Sandra Rother[6], Claudia Schirra[1,2], Yvonne Schwarz[7], Elmar Krause[1], Walter J. Schulz-Schaeffer[8], Veit Flockerzi[9], Chi-Kuang Yao[10,11], Hsin-Fang Chang*[1,2,12]

1. Cellular Neurophysiology, Center for Integrative Physiology and Molecular Medicine (CIPMM), Saarland University, 66421 Homburg, Germany
2. Center for Gender-specific Biology and Medicine (CGBM), University of Saarland, 66421 Homburg, Germany
3. Department of Neurology, Saarland University, 66421 Homburg, Germany
4. Department of Pathology, Saarland University, 66421 Homburg, Germany
5. Medical Biochemistry and Molecular Biology, Saarland University, 66421 Homburg, Germany.
6. Biophysics, Center for Integrative Physiology and Molecular Medicine (CIPMM), Saarland University, 66421 Homburg, Germany
7. Institute for Physiology, Center of Integrative Physiology and Molecular Medicine (CIPMM), Saarland University, Homburg, Germany.
8. Institute for Neuropathology, Medical Faculty, Saarland University, 66421 Homburg, Germany
9. Experimental and Clinical Pharmacology and Toxicology, Center for Molecular Signaling (PZMS), Saarland University, Building 46, 66421 Homburg, Germany.
10. Neuroscience Program of Academia Sinica, Academia Sinica, Taipei, Taiwan
11. Institute of Biochemical Sciences, College of Life Science, National Taiwan University, Taipei, Taiwan
12. Department of Medicinal and Applied Chemistry, Kaohsiung Medical University, 100 Shih-Chuan 1st Road, 80708 Kaohsiung, Taiwan

* Correspondence should be addressed to Dr. Hsin-Fang Chang Hsin-Fang.Chang@uks.eu

Abstract

Flower isoforms regulate cellular fitness and are implicated in neurodegeneration and tumor progression, yet their mechanisms remain unclear. Using Flower knockout mice, we identify the N- and C-terminal domains as distinct signaling modules: the C-terminus promotes survival of fitter ('winner') cells via intrinsic signaling, while the N-terminus induces apoptosis of neighboring less-fit ('loser') cells via extrinsic signaling. Notably, Flower signaling operates via secreted extracellular vesicles (EVs), with the 'win' isoform exhibiting ~25-fold higher secretion than the 'lose', thereby facilitating intercellular fitness selection. In Alzheimer's disease human brain tissue and APP transgenic mice, win isoforms are enriched in astrocytes near amyloid-β plaques, suggesting localized fitness surveillance. In cortical neuron-glia cultures, overexpression of the win isoform or its C-terminal domain enhances astrocytic Aβ clearance and protects neurons from Aβ toxicity. These findings uncover a novel Flower signaling pathway controlling cell death, providing new insights into EV-mediated communication with therapeutic potential in neurodegeneration.

Introduction

The *Flower* gene was first identified in *Drosophila melanogaster*, where mutations impaired synaptic vesicle endocytosis and led to distinctive “flower-like” synaptic boutons at neuromuscular junctions[1]. Subsequent studies have confirmed Flower's role in endocytosis in both invertebrates and vertebrates[1, 2, 3, 4, 5]. *Flower* is evolutionarily conserved from flies to mammals and is ubiquitously expressed across tissues, highlighting its ancient and essential biological functions. The gene encodes multiple isoforms, some of which are involved in calcium channel activity and vesicle trafficking[1, 3, 6, 7, 8, 9]. More recently, specific Flower isoforms have been recognized as key regulators of a fundamental process known as cellular fitness competition[10, 11], a natural selection mechanism that eliminates unfit cells by inducing apoptosis while allowing healthy, fit cells to continue growing[12, 13, 14]. This selection process results in the survival of fitter cells, so-called ‘winners’, while unfit cells die, making them the ‘losers’.

In heterogeneous cell populations, Flower isoforms function as molecular "fitness fingerprints" displayed on the cell surface[10, 11]. Fit cells predominantly express “win” isoforms, while less-fit cells express “lose” isoforms. This differential expression drives selective apoptosis of unfit cells and survival of fitter neighbors, establishing a winner–loser signaling axis. Such fitness-based cell selection is essential for tissue integrity during embryonic development, aging, infection, tumorigenesis, and neurodegeneration[15, 16, 17, 18, 19, 20, 21, 22]. Despite its broad relevance, the mechanistic basis of Flower-mediated signaling in mammals remains poorly understood.

Tissue homeostasis depends on maintaining a balanced fitness landscape. Pathological states such as neurodegeneration disrupt this balance, generating heterogeneous cell populations with divergent fitness. Understanding how Flower isoforms modulate cell survival and elimination may offer a novel strategy to selectively preserve functionally competent cells while removing compromised ones.

In the context of Alzheimer’s disease (AD), this concept gains particular significance. Astrocytes play a central role in maintaining brain homeostasis and clearing amyloid-β (Aβ) aggregates[23, 24, 25, 26, 27]. However, their role is dual-edged: while they can facilitate Aβ clearance, they may also exacerbate pathology through chronic activation and impaired degradation. Astrocytic responses are highly heterogeneous[28, 29], and this plasticity suggests that they may also participate in fitness-based cellular competition.

Here, we investigate the domain-specific roles of Flower isoforms in regulating cellular fitness in the adult brain. Using Flower knockout (KO) mice, molecular expression analyses, and Aβ toxicity assays in cortical neuron–glia cultures, we demonstrate that the N-terminal and C-terminal domains of Flower mediate distinct signaling outcomes, apoptosis of unfit cells and intrinsic survival promotion, respectively. Importantly, we show for the first time that Flower, secreted via extracellular vesicles (EVs), participates in the signaling process that regulates cellular fitness, a mechanism previously thought to occur solely through direct cell–cell contact between neighboring cells. Moreover, in amyloid-precursor-protein (APP) transgenic mice and human AD brain tissue, we observe high expression of “win” Flower isoforms in astrocytes surrounding Aβ plaques, suggesting localized

activation of Flower-mediated fitness surveillance in neurodegeneration. These findings uncover a previously unrecognized mechanism of intercellular fitness signaling and suggest Flower isoforms as potential therapeutic targets in neurodegenerative disease.

Results

Localized upregulation of Flower win isoforms in astrocytes near amyloid plaques in the neocortex

To study Flower's role in cellular fitness during neurodegeneration, we used the APP transgenic mouse model of AD, which develops early amyloid plaques. Given the cytotoxicity of amyloid plaques[30, 31], we hypothesized that surrounding cells exhibit heterogeneous fitness states, potentially modulated by Flower-mediated signaling.

We first quantified Flower gene expression in plaque-associated regions. Cortical brain sections from APP mice were stained with Congo Red to visualize amyloid plaques, and plaque-adjacent regions were isolated via laser capture microdissection. Cortical regions lacking plaques served as controls. RNA extracted from these areas was analyzed by quantitative RT-PCR, revealing a significant upregulation of Flower splice variants (mFwe1–3) in plaque-associated regions compared to non-plaque controls, indicating locally elevated Flower signaling at sites of pathology (Fig. 1a). In contrast, total *Flower* gene expression in whole-brain lysates of APP mice remained unchanged relative to wild-type (WT) mice, suggesting that Flower upregulation is spatially restricted (Fig. 1b).

Given the known role of glial cells in plaque clearance[32, 33], we next investigated which glial populations express high levels of Flower protein. We focused on the "win" isoforms of Flower, which serve as molecular signatures of fitter cells. Mouse Flower encodes four isoforms (Fig. 1c); among them, mFwe1 and mFwe3 are associated with "loser" phenotypes, whereas mFwe2 and mFwe4 correspond to "winner" phenotypes[34]. Importantly, the win isoforms contain a C-terminal domain absent in the lose isoforms. To detect these selectively, we used a custom, sequence-specific antibody (#C1557) targeting the unique C-terminal epitope of the win isoforms.

We confirmed the enrichment of Iba1$^+$ microglia and GFAP$^+$ astrocytes around amyloid plaques (Fig. 1d). Co-staining of glial markers and the Flower win isoforms allowed us to quantify Flower-high cells in both plaque-associated and plaque-distant regions (Fig. 1e–f). Plaque proximity was defined as within ~50 µm from the plaque edge, visualized by Thioflavin S (ThioS) staining. All astrocytes and microglia within the imaged fields were counted, and their Flower win expression was categorized as high or low based on visibility under identical imaging conditions. Among all analyzed glial populations, approximately 45% of astrocytes in plaque-associated regions exhibited high Flower win expression, compared to only 7% in non-plaque areas. In contrast, only ~4% of microglia near plaques expressed high levels of Flower win, while this proportion dropped to 0.5% in more distal regions. Overall, Flower win expression was markedly more prominent in astrocytes than in microglia (Fig. 1g).

To validate these findings in human tissue, we analyzed postmortem cortical sections from AD patients. Consistent with our observations in the mouse model, we found an accumulation of astrocytes near amyloid plaques (Fig. 1h-i). Using the same C-terminal Flower antibody, we observed that approximately 45% of astrocytes in plaque-associated regions expressed high levels of

Flower protein, compared to only 7% in non-plaque areas (Fig. 1j). A subset of astrocytes showed no detectable Flower staining, suggesting a heterogeneous astrocyte population in the brain. However, due to species-specific sequence differences, the antibody does not exclusively recognize human "win" isoforms, but rather detects Flower protein variants independently of their fitness phenotype. Nonetheless, quantification revealed a significantly higher proportion of Flower$^+$ astrocytes near plaques, supporting the clinical relevance of Flower expression in AD pathology (Fig. 1j).

These results suggest a localized upregulation of Flower win isoforms in astrocytes near amyloid plaques, highlighting a potential role for Flower-mediated fitness signaling in glial responses to pathology. Based on these findings, we selected astrocytes as the primary cell type to dissect Flower's functional role in cellular fitness regulation in the context of AD.

Flower isoforms mediate differential cell survival in primary astrocytes

To investigate how Flower regulates cell fate, we first established a cellular fitness assay using primary astrocytes derived from Flower knockout (KO) mice. Based on the known classification of mouse Flower isoforms as "win" (mFwe2 and mFwe4) or "lose" (mFwe1 and mFwe3) isoforms[34], we reintroduced these specific isoforms via electroporation to generate distinct 'winner' and 'loser' astrocyte populations.

Astrocytes transfected with specific Flower isoforms were subsequently co-cultured in pairwise combinations to assess cell–cell interactions. Both homotypic (mFwe1+ mFwe1, mFwe2+ mFwe2, mFwe3+ mFwe3) and heterotypic (mFwe1+ mFwe2, mFwe1+ mFwe3, mFwe1+ mFwe4, mFwe2+ mFwe1, mFwe2+ mFwe3, mFwe2+ mFwe4, mFwe3+ mFwe4) combinations were analyzed, enabling classification into win–win, lose–lose, and win–lose groups (Fig. 2a). After 24 h of co-culture, we observed dynamic interactions between cells, particularly in heterotypic pairings. Confocal imaging revealed sustained contacts as well as selective cell elimination. Cell death was assessed using two complementary approaches: pre-fixation application of the membrane-impermeable dye DAPI to label cells with compromised membranes, and post-fixation immunostaining for cleaved caspase-3 (CC3) to detect apoptosis (Fig. 2b). Cell–cell contact pairs were analyzed to determine viability. Dead cells included both early apoptotic (CC3$^+$) and late apoptotic or necrotic (DAPI$^+$ with nuclear fragmentation) phenotypes.

In heterotypic co-cultures of win and lose isoforms, approximately 45% of cells expressing lose isoforms underwent cell death, whereas winner cells remained largely unaffected. In contrast, homotypic cultures exhibited minimal cell death (6–8%) (Fig. 2c). Notably, in co-cultures such as Fwe1 + Fwe2, Fwe2 + Fwe3, Fwe3 + Fwe4, and Fwe1 + Fwe4, cells expressing Fwe1 or Fwe3 consistently underwent selective elimination, confirming their functional identity as "loser" isoforms. Overall, 35–45% of less-fit (loser) cells were eliminated via Flower-mediated cell competition (Fig. 2d).

To further validate our fitness assay, we tested human Flower isoforms hFwe3 ("lose") and hFwe4 ("win"), whose phenotypes have previously been characterized in tumor models[16]. Consistent with the cell selection observed in mouse Flower, homotypic cultures of win–win (hFwe4 + hFwe4) or lose–

lose (hFwe3 + hFwe3) combinations resulted in minimal cell death among the cell–cell contact. However, co-culture of hFwe3- and hFwe4-expressing astrocytes led to approximately 40% total cell death in the mixed population (Extended Data Fig. 1a, b), with ~40% of hFwe3-expressing cells selectively eliminated (Extended Data Fig. 1c).

In summary, we established a primary astrocyte co-culture assay that reliably recapitulates Flower-mediated elimination of less fit ("loser") astrocytes by fitter ("winner") counterparts, while homotypic cultures remain unaffected. These results validate our assay as a robust platform for studying Flower-driven fitness signaling between glial cells.

N- and C-termini of Flower isoforms localize to the cytoplasmic side in astrocytes

Cellular fitness is generally considered to be regulated via cell–cell contact[11], implying that the functional domains of Flower isoforms should be exposed on the cell surface. However, topological predictions for full-length mouse Flower isoforms are inconsistent with experimental observations[4, 34].

To resolve this inconsistency, we examined the membrane orientation of the N- and C-termini of mFwe1 and mFwe2, the dominant 'lose' and 'win' isoforms, in primary mouse astrocytes. To assess topology, we employed pHluorin2, a pH-sensitive GFP variant, fused to either the N- or C-terminus of each isoform. WT astrocytes were transfected with these constructs, and live-cell confocal imaging was performed to monitor ratiometric fluorescence (405/488 nm) in response to cytosolic acidification induced by the ionophore Carbonyl cyanide m-chlorophenyl hydrazone (CCCP). During imaging, astrocytes were maintained in DMEM; CCCP-induced acidification was driven by proton release from intracellular vesicles and mitochondria. DMSO-treated cells served as vehicle controls. As localization references, cytosolic pHluorin2 and vesicle-luminal Synaptobrevin2–pHluorin2 (Syb2–pHluorin2) were included.

Upon CCCP treatment, cytosolic pHluorin2-expressing cells exhibited a reduced 405/488 ratio, confirming effective cytoplasmic acidification (Fig. 3a). Both N- and C-terminally tagged mFwe1 constructs showed similar decreases in fluorescence ratio (Fig. 3b–c), indicating that both termini are localized to the cytoplasmic side. In contrast, Syb2–pHluorin2, residing within vesicle lumens, remained unaffected by CCCP treatment (Fig. 3d). Notably, mFwe2 constructs tagged at either terminus also displayed a similar decrease in fluorescence ratio upon CCCP treatment (Fig. 3e–f), arguing cytoplasmic localization of both N- and C-termini of mFwe2. To further validate the localization of Flower in astrocytes, we used lentiviral transduction to express mFwe2 isoform as dominated isoform in WT cells, thereby limiting overexpression artifacts caused by excess plasmid-derived protein. Consistent with previous report, lentivirally expressed mFwe2 exhibited a vesicular distribution, consistent with its classification as a vesicular membrane protein[1] (Fig. 3g).

These findings demonstrate that in astrocytes, both the lose isoform mFwe1 and the win isoform mFwe2 possess cytoplasmic regulatory domains. This orientation challenges the prevailing model of Flower-mediated cellular fitness as a contact-dependent process[11] and instead suggests an alternative signaling mechanism.

Secreted Flower-carrying vesicles convey fitness signals to eliminate unfit cells

While Flower homologs share certain structural similarities, the C-terminus of Drosophila Flower, located extracellularly, has been shown to regulate cellular fitness[11]. In contrast, although the mouse Flower protein also possesses non-membrane-embedded domains at both the N- and C-termini, our data confirm that both termini are oriented toward the cytoplasm. This finding challenges the model in which Flower functions as a cell surface code for fitness recognition. We hypothesize that Flower may instead be secreted from astrocytes via an alternative mechanism through extracellular vesicles. Supporting this, we detected extracellular Flower signals using the Flower antibody (#C1557) in brain tissue from both APP-transgenic mice and AD patients (Fig. 4a). To investigate the mechanism of secretion, we performed Western blot analysis on Flower KO astrocytes overexpressing Flag–Flower–HA constructs. All isoforms showed cleavage fragments detected by anti-Flag (N-terminus) and anti-HA (C-terminus) antibodies. Anti-Flag revealed multiple bands for all isoforms, with mFwe2 comprising ~40% full-length and ~60% cleaved protein, while other isoforms remained predominantly full-length (70–80%) (Extended Data Fig. 2a). Similar banding patterns were seen with anti-HA, particularly for mFwe2; however, small fragments (<10 kDa) may have escaped detection due to technical limitations (Extended Data Fig. 2b). Reprobing with a polyclonal Pan-Flower antibody[4] that recognizes both termini confirmed that these bands correspond to Flower protein (Extended Data Fig. 2c).

To explore whether Flower fragments are secreted. EVs were isolated from the supernatants of WT and Flower-overexpressing WT astrocyte cultures by 100,000 × g ultracentrifugation. Immunostaining with the anti-Pan-Flower antibody showed Flower-positive puncta in both WT and mFwe2-pHluorin2 cultures (Fig. 4b). Structured illumination microscopy (SIM) revealed that ~20% of these puncta co-localized with the membrane dye DiD, while ~80% did not, suggesting most secreted Flower might not be membrane-bound (Fig. 4c).

To assess isoform-specific secretion, we analysed supernatants from astrocyte cultures expressing either the mFwe2 (“win”) or mFwe1 (“lose”) isoform, each tagged with Flag and HA at the N- and C-termini, respectively (Fig. 4d, e). Structured illumination microscopy (SIM) revealed both double- and single-positive Flower puncta, indicating the presence of full-length proteins as well as cleaved N- and C-terminal fragments associated with individual EVs (Extended Data Fig. 2d). Western blot analysis of isolated EVs confirmed the presence of both mFwe1 and mFwe2, as detected by anti-Flag, anti-HA, and pan-Flower antibodies (Fig. 4f).

To compare the levels of secreted Flower between isoforms, 10 μg of EV protein per group was analysed by western blot. The anti-Flag blot was selected for quantification due to its high specificity and consistent performance within the linear detection range. Band intensities were quantified and normalised to the number of transfected cells. Astrocytes expressing mFwe2 secreted approximately 25-fold more Flower protein than those expressing mFwe1, revealing isoform-specific differences in EV-associated release (Fig. 4g). To calculate the amount of secreted protein, we quantified the number of transfected primary astrocytes expressing either mFwe1–mCherry or mFwe1–mTFP

("lose"), and mRFP–mFwe2 or mFwe2–mTFP ("win") constructs. Each transfection was performed using 4×10^6 cells and 5 μg of Fwe plasmid. Transfection efficiency was assessed by confocal imaging, showing a higher efficiency for mFwe2 (51%) compared to mFwe1 (42%) (Extended Data Fig. 3a). Despite this difference, fluorescence intensity per cell was comparable between isoforms, indicating similar expression levels at the single-cell level (Extended Data Fig. 3b).

To test the functional relevance of the secreted material, 1×10^5 unfit astrocytes (transfected with mFwe1–mCherry) were treated with ~10 μg of EVs derived from WT, mFwe1-, or mFwe2-expressing cells. Cell death was assessed by CC3 and DAPI staining. Only EVs derived from mFwe2-expressing astrocytes induced a significant increase in cell death (>30%) (Fig. 4h–j), whereas EVs from WT or mFwe1-expressing cells had no significant effect, likely due to lower levels of secreted Flower.

Together, these results demonstrate that Flower, primarily in its 'win' isoform, is secreted via EVs or EV-like vesicles. Full-length and cleaved Flower fragments exist in both membrane-bound and soluble forms and are capable of transmitting fitness signals that drive the selective elimination of unfit cells. This reveals a previously unrecognized mechanism of Flower-mediated intercellular communication via EVs, distinct from the classical model of direct cell–cell contact.

Flower's N-terminus induces apoptosis, while its C-terminus confers survival

To identify functional regions of Flower involved in fitness signaling, we focused on three domains containing potential interaction motifs: the N-terminus (YxxL)[35], exon 3 (conferring a win phenotype in human cells)[16], and the C-terminus (YxxI)[36] (Fig. 5a). Since Flower acts as a cellular fitness code, we hypothesized that interactions mediated by these signal domains trigger intercellular signals regulating survival or apoptosis. To test this, we engineered truncated Flower domains fused to mScarlet I and a platelet-derived growth factor receptor (PDGFR) transmembrane domain (mFwe-mScarlet I-TM) to localize them extracellularly to the plasma membrane (Extended Data Fig. 4a). Proper surface expression in astrocytes was confirmed by RFP and HA staining under non-permeable conditions (Extended Data Fig. 4b). These constructs were then expressed in Flower KO astrocytes and separately co-cultured with mFwe2 (fit) or mFwe1 (unfit) cells to assess cell death (Fig. 5b).

Our results revealed that the N-terminal domain of Flower induced apoptosis specifically in unfit cells when co-cultured with fit cells, while fit cells were unaffected (Fig. 5c,d and Extended Data Fig. 4c). To determine whether this signaling was directly dependent on the truncated Flower peptide or required additional molecular partners, we applied synthetic peptides derived from the truncated Flower domains to the cells (Fig. 5e). Consistent with the cell-based experiments, the synthetic N-terminal peptide induced apoptosis in unfit cells but not in fit cells (Fig. 5f). Furthermore, the synthetic N-terminal peptide exhibited a dose-dependent effect, with cell death in unfit populations reaching approximately 35%, mirroring observations from cellular co-culture assays expressing Flower (Fig. 5g).

Given that the mFwe win isoforms contain a distinct C-terminal domain, we hypothesized that this domain promotes cell survival and confers the winner phenotype (Fig. 2a). To test this, we attempted to rescue unfit cells by co-transfecting them with mFwe1 or mFwe3 along with a C-terminal-TM

construct. Co-expression of the C-terminal domain significantly reduced apoptosis in cells treated with N-terminal peptides (Fig. 5h,i). Overexpression of the C-terminal domain of Flower in unfit cells did not alter cell survival, suggesting that the rescue phenotype driven by the C-terminal domain is due to the alteration of intrinsic cellular death mechanisms, rather than a direct effect on promoting cell survival (Extended Data Fig. 5a,b). This finding strongly supports the notion that the N- and C-terminal domains of Flower regulate cellular fitness oppositely: the N-terminus induces apoptosis in unfit cells, while the C-terminus mitigates death signaling.

To further elucidate the molecular pathways involved, we analyzed the expression of key apoptosis-related genes, Caspase3, Bax, and Bcl2 in unfit (mFwe1-expressing) cells co-expressing the Flower C-terminal domain. Treatment with the N-terminal peptide led to upregulation of *Caspase3* and *Bax*, consistent with apoptotic activation. In contrast, overexpression of the C-terminal domain resulted in their downregulation, while Bcl2 levels remained unchanged, suggesting that Flower-mediated cell death primarily involves the Caspase3–Bax axis (Fig. 5j).

Together, these findings define the opposing functions of Flower's terminal domains in regulating cellular fitness: the N-terminus promotes apoptosis in unfit cells, while the C-terminus counteracts this signal. This highlights a finely tuned mechanism of cell competition through dual-domain regulation.

Flower signaling promotes astrocytic clearance of Aβ protofibrils and neuronal survival

To study Flower-mediated cell fitness in amyloid pathology, we established an amyloidogenic neuron–glia co-culture model mimicking Aβ accumulation and toxicity in Alzheimer's disease. Brain cortical cells from WT mouse pups were cultured and treated with Aβ protofibrils. Immunostaining confirmed that astrocytes comprised ~90% of the glial population. Aβ42 monomers were pre-incubated for 4 h at 37°C incubator to form protofibrils, which are known to induce cytotoxicity[31, 37]. Cortical neuron–glia cultures were infected on day 1 in vitro (DIV1) with lentiviral constructs expressing either the Flower win isoform (mFwe2), the Flower C-terminal signaling domain, or mScarlet I as a control. On DIV7, cultures were treated with Alexa647-conjugated Aβ protofibrils (0.1 μM) and maintained for six days to assess Aβ-induced cytotoxicity. To assess cytotoxicity, cells were fixed and stained with CC3 antibody (Fig. 6a). Confocal imaging showed that Aβ protofibrils significantly increased apoptosis, with ~45% CC3+ neurons and ~35% CC3+ astrocytes. However, overexpression of either mFwe2 or the cytosolic Flower C-terminal domain markedly reduced CC3+ cells to baseline levels, comparable to untreated controls (Fig. 6b).

Interestingly, we observed changes in the size and abundance of Aβ protofibrils in these cultures. Since astrocytes can phagocytose Aβ aggregates[38], we hypothesized that Flower enhances this clearance, thereby reducing toxicity and supporting neuronal survival. To test this, cultures were trypsinized to isolate surviving glial cells, and intracellular Aβ protofibril levels were analyzed by flow cytometry. FACS data showed ~60% of WT cells were positive for Aβ protofibrils-Alexa647, whereas ~75% of cells overexpressing mFwe2 or the Flower C-terminal domain showed increased uptake (Fig. 6c, d).

Confocal quantification showed reduced Aβ protofibril size in mFwe2-overexpressing cultures (mean: 3 μm^2; median: 0.4 μm^2) compared to WT controls (mean: 6 μm^2; median: 1 μm^2), with no change in C-terminal domain-overexpressing cultures (Fig. 6e). Size distribution analysis revealed that mFwe2 specifically reduced larger protofibrils (Fig. 6f, a; right panel), indicating distinct mechanisms from the C-terminal domain, despite both enhancing cell survival. Together, these results demonstrate that Flower-mediated signaling, especially the C-terminal domain, enhances astrocytic clearance of amyloid-beta aggregates and promotes neuronal survival by reducing cytotoxicity in Alzheimer's disease-like pathology.

Direct N–C terminal interaction suppresses pro-apoptotic signaling

To investigate how the opposing roles of Flower's signaling domains regulate cell fitness, we hypothesized that the protective function of the C-terminus may involve in a direct interaction with the pro-apoptotic N-terminal region. We performed surface plasmon resonance (SPR) assays by immobilizing the synthetic C-terminal peptide on the chip and injecting either the N-terminal or C-terminal peptide as control to assess binding. The results demonstrated a specific, concentration-dependent interaction between the N- and C-terminal regions, while no binding was observed between C-terminal peptides alone (Extended Data Fig. 6a, b).

These findings support a model in which Flower functions as a modular signaling platform: the N-terminal domain promotes apoptosis in unfit cells, while the C-terminal domain counteracts this effect through direct binding. This intramolecular Flower interaction serves as a regulatory mechanism that modulates the balance between elimination and survival signals within the tissue environment.

Based on our results, we propose a model for how Flower regulates cellular fitness (Fig. 7). Flower, as a membrane protein, resides on vesicles with both its N- and C-termini oriented toward the cytoplasm. This orientation is preserved when these vesicles fuse with the plasma membrane. Since both N- and C-terminal–tagged Flower fragments were detected in EVs isolated from culture supernatants, their origin likely traces back to intracellular organelles that package these EVs. Although the exact vesicle type remains unclear, proteolytic cleavage of Flower likely occurs within these organelles.

The secreted EVs carrying Flower N-terminal fragments mediate the removal of unfit cells. In contrast, overexpression of the C-terminal domain, anchored to the plasma membrane (Fwe C-TM), directly binds the N-terminus and neutralizes its pro-apoptotic signaling. This suppresses the activation of apoptotic gene expression and confers intrinsic protection to the cell.

Discussion

Our study identifies a previously unrecognized mechanism by which Flower isoforms regulate astrocyte fitness in the context of amyloid pathology. Notably, this regulation is mediated by secreted EVs, challenging the prevailing model that Flower-dependent fitness signaling relies exclusively on direct cell–cell contact. Given the conserved nature of fitness surveillance across development and disease contexts[12, 13, 15, 19, 39, 40], our findings may extend beyond neurodegeneration to other settings such as tumor biology[16, 41], where cell competition and selective survival also shape tissue dynamics.

Mechanistically, we show that Flower encodes both pro-apoptotic and pro-survival cues within a single transmembrane protein. The N-terminal domain promotes cell death, while the C-terminal domain physically interacts with and neutralizes this pro-death signal. This intramolecular antagonism enables fine-tuned regulation of cell fate within the same molecule, distinguishing Flower from multifunctional proteins like p53, Notch, or Bcl-2 family members[42, 43, 44, 45, 46], which typically rely on alternative splicing, post-translational modifications, or distinct interaction partners to mediate opposing functions. Flower's intrinsic duality thus provides a modular framework for autonomous control of cellular fitness, with broad implications for tissue homeostasis and therapeutic targeting.

An intriguing observation is that Flower-mediated elimination of unfit astrocytes consistently reaches only ~35–40%, regardless of whether triggered by cell–cell competition, synthetic peptide application, or treatment with Flower-containing EVs. This partial response likely reflects intrinsic heterogeneity within the astrocyte population, suggesting that Flower-dependent death signaling may be restricted to a specific subpopulation or activated only under defined cellular states.

The selective upregulation of Flower win isoforms in plaque-associated astrocytes suggests an active role in modulating survival decisions during neurodegenerative stress. Whether these Flower-high astrocytes gain a competitive advantage or exert paracrine effects via EVs remains unclear. However, our data show that win isoforms are secreted at significantly higher levels than lose isoforms and promote neuronal viability, likely by modulating the glial environment. Moreover, win isoform overexpression enhances Aβ protofibril uptake in astrocytes, raising the possibility that Flower also influences amyloid clearance or deposition. In mixed neuron–glia cultures, Flower win isoforms or the C-terminal domain conferred robust neuroprotection during Aβ exposure, likely through selective enrichment of fit, Flower-expressing cells over time. These findings position Flower as a key mediator linking fitness signaling to glial support in Alzheimer's disease.

While our in vitro fitness assays were conducted using overexpression systems in Flower knockout cells, they raise an important question for future investigation: how do heterogeneous cell populations in vivo regulate Flower isoform expression to enforce competitive survival outcomes? In particular, elucidating the transcriptional or post-transcriptional mechanisms that tip the balance toward "win" or "lose" isoform expression may provide insight into how tissue-level homeostasis is maintained or disrupted in disease.

Our findings also challenge long-standing assumptions regarding Flower's topology and mode of action. Although previously proposed to act via surface-exposed domains that distinguish winners

from losers[10, 11], we demonstrate using pH-sensitive tags that both N- and C-termini are cytoplasmic in intact cells. Surprisingly, Flower undergoes proteolytic cleavage and is secreted as membrane-associated and non-membrane-associated fragments, enabling non-cell-autonomous signaling. The pro-apoptotic N-terminal domain is exposed on secreted particles, providing a mechanistic basis for how intracellular Flower domains exert extracellular effects. Importantly, this paracrine-like mechanism allows Flower to influence fitness beyond direct contact, through unconventional EV-like carriers.

The secretion pathway underlying Flower release appears atypical. Most secreted Flower fragments did not co-localize with the lipophilic dye DiD, suggesting they are not associated with classical lipid-rich EVs. As a transmembrane protein, this raises the possibility that Flower is secreted via a non-canonical route, such as through low-lipid vesicles, partial membrane fragments, or a yet uncharacterized class of fitness-associated vesicles. This unconventional secretion may reflect specialized trafficking, as observed for the human isoform hFWE4, which localizes to lamellar body-like vesicles in keratinocytes[47]. There, Flower triggers Ca^{2+} release to regulate surface cargo delivery, a process critical for skin barrier formation. Analogously, mFwe2 may exploit a similar, context-specific secretory mechanism in glia.

The presence of the N-terminal “death signal” in both win and lose isoforms raises an apparent paradox in fitness discrimination. However, we found that win isoforms (mFwe2) are secreted ~30-fold more than lose isoforms (mFwe1), despite comparable total protein levels. This suggests that differential trafficking and sorting, potentially driven by structural differences between isoforms, underlies the selective release of pro-survival signals, enabling “winner” cells to eliminate less fit neighbors. Such a mechanism would confer a survival advantage while maintaining tissue integrity under stress.

Downstream, we identify the Caspase-3–Bax axis as the primary effector of Flower-mediated apoptosis. Despite robust activation of this pathway, Bcl2 levels remained unchanged, suggesting that Flower bypasses traditional anti-apoptotic checkpoints, possibly via direct Bax activation or upstream modulation of mitochondrial membrane permeabilization[48, 49]. This provides a mechanism by which fitness-induced apoptosis can proceed even in survival-favoring environments.

Taken together, our findings establish Flower as a critical regulator of astrocyte fitness and neuronal survival in Alzheimer’s disease. Through isoform-specific functions and an unexpected EV-based mode of intercellular signaling, Flower orchestrates competitive fitness decisions that shape glial responses to neurodegenerative stress. This non-canonical form of extracellular communication reveals a broader paradigm in which tissue-level competition influences disease progression. By refining the conceptual framework of glial involvement in AD, our work positions Flower as a promising therapeutic target for preserving brain homeostasis and mitigating neuronal loss.

Materials and Methods

Mice

Fwe KO mice were generated as previously described[4]. APP/PS1 transgenic mice (APP^{tg}), which overexpress human mutated APP (KM670/671NL) and PS1 (L166P) under the control of Thy1 promoters (PMC1559665), were kindly provided by M. Jucker (Hertie Institute for Clinical Brain Research, Tübingen, Germany). All transgenic and WT mice used in this study were on a C57BL/6N background. Fwe KO pups used for astrocyte isolation were postnatal day 0–2 (P0–P2). Adult WT and APP mice used for brain tissue staining and RNA analysis were 60-70 weeks old and included both sexes. Animals were housed at 22 °C with 50–60% humidity under a 12 h light/dark cycle. All experimental procedures were approved by the local regulatory authority of Saarland (Landesamt für Verbraucherschutz; protocols AZ: 2.4.1.1/11-2021 to E.K. and VM2023-05 to Y.L.) and carried out in accordance with institutional and governmental guidelines.

Flower antibody generation

Details of Flower antibody generation have been previously described[4]. In this study, two custom-made polyclonal antibodies were used. The first, referred to as Flower antibody #1557, was sequence-directed and raised against the C-terminal 18 amino acids shared by mFwe2 and mFwe4. The second, a pan-Flower antibody, was generated against the full-length recombinant mFwe2 protein[4] and recognizes multiple epitopes across the Flower protein, including both N- and C-terminal regions.

Peptides synthesis

Peptides were synthesized with an automated ResPepSL synthesiser (Intavis) using amide Rink resin as the solid phase and Fmoc-protected amino acids (Carbolution) for coupling according to the method of Merrifield[50]. The resin-coupled peptides were cleaved and deprotected with trifluoroacetic acid (Sigma Aldrich) followed by precipitation with tert-butyl methyl ether (Fisher Scientific) and further analysis and purification by preparative HPLC (Merck) (purtity > 90%). Lyophilized peptides (Lyovac GT2, Finn-Aqua) were stored at 4 °C. Stock solutions of the peptides were prepared fresh and used the same day.

Mouse brain slice preparation and staining

APP-transgenic mice and age-matched WT littermates were sacrificed by CO_2 inhalation followed by decapitation. Brains were extracted and post-fixed in 4% paraformaldehyde (PFA) at 4 °C for 24 h. Fixed tissues were sectioned into 30 µm slices using a vibratome (Leica VT1000 S). Sections were washed three times with Dulbecco's PBS (D-PBS), permeabilized with 0.1% Triton X-100 for 10 min, and blocked with 10% fetal calf serum (FCS) for 30 min at room temperature (RT). Primary antibodies

were applied overnight at 4 °C, followed by incubation with Alexa Fluor-conjugated secondary antibodies. Nuclei were counterstained with DAPI, and slices were mounted and imaged by confocal microscopy.

Immunostaining of postmortem human brain sections from AD patients

Formalin-fixed, paraffin-embedded hippocampal sections from autopsy-confirmed Alzheimer's disease (AD) patients were obtained from the Department of Neuropathology, Saarland University, Germany. The use of human tissue was approved by the Ärztekammer des Saarlandes (Ethics Committee of the Medical Association of Saarland), approval number 106/25. Following deparaffinization, slides were subjected to antigen retrieval in citrate buffer (pH 6.0) for 30 min. Endogenous peroxidase activity was quenched with 3% H_2O_2 in PBS, and sections were blocked for 1 h in 0.2% casein.

Immunostaining was performed using a rabbit polyclonal anti-GFAP antibody (1:500, Z0334; DAKO, Agilent Technologies, Waldbronn, Germany), followed by detection with an alkaline phosphatase (AP)-conjugated goat anti-rabbit IgG secondary antibody (DAKO) and visualization using the Vector Red Substrate Kit (SK-5100; Vector Laboratories, Newark, USA).

To assess astrocytic localization of Flower protein, serial sections were stained with a rabbit polyclonal anti-Flower antibody, followed by GFAP staining. Detection was performed with either AP- or horseradish peroxidase (HRP)-conjugated goat anti-rabbit IgG secondary antibodies (both from DAKO), and developed with either 3,3'-diaminobenzidine tetrahydrochloride (DAB; Sigma) or the Vector® Blue Substrate Kit (SK-5300; Vector Laboratories). Slides were counterstained with hematoxylin.

For fluorescence-based colocalization analysis, the same staining protocol was repeated using Alexa Fluor 488- or Cy3-conjugated goat anti-rabbit IgG secondary antibodies (Jackson ImmunoResearch Europe Ltd, Cambridgeshire, UK). Colocalization between Flower and GFAP was evaluated by confocal microscopy (LSM 780, Zeiss).

Primary cortical neuron and astrocyte culture

Cortical neurons and astrocytes were isolated from P0–P2 mouse pups. Cerebral hemispheres were dissected in ice-cold Earle's Balanced Salt Solution (EBSS; Gibco). Following removal of the meninges, cortices were minced into small fragments and enzymatically digested with 35 U/mL papain (Worthington) at 37 °C for 45 min, followed by gentle mechanical trituration to obtain a single-cell suspension. For neuronal culture, dissociated cells were seeded onto 25 mm glass coverslips placed in 6-well culture plates at a density of 3×10^5 cells per coverslip. Coverslips were pre-coated with a solution containing 17 mM acetic acid, collagen I (Gibco), and poly-D-lysine (Sigma). On day in DIV 1, the culture medium was replaced to remove residual debris. Neurons were maintained in Neurobasal-A (NBA) medium supplemented with 10% FCS, 1% penicillin-streptomycin (Invitrogen), 1% GlutaMAX, and 2% B27 supplement (Gibco). Neurons were cultured for 9–12 days prior to

experimental use. For astrocyte culture, dissociated cortical cells were seeded into T-75 culture flasks (one brain per flask), pre-coated with poly-L-ornithine (Sigma). On DIV1, flasks were rinsed and vigorously agitated with DPBS to remove debris and non-adherent cells. The remaining adherent astrocytes were cultured in Dulbecco's Modified Eagle Medium (DMEM; Gibco) supplemented with 10% FCS and 1% penicillin-streptomycin for 9–14 days before use in experiments.

Cell fitness assay

To assess the fitness effects of Flower isoforms, Flower KO astrocytes cultured for 9–12 days were used. Cells were detached using Trypsin-EDTA, washed three times with DPBS, and resuspended in 100 µL nucleofection solution (Basic Nucleofector Kit for Primary Mammalian Glial Cells, Lonza). Each nucleofection was performed with 4×10^6 astrocytes and 5 µg plasmid DNA encoding fluorescently tagged win or lose Flower isoforms. Electroporation was carried out using a electroporation device (Lonza NucleofectorI/II/2b System). Following electroporation, equal numbers of the two transfected astrocyte populations were mixed and co-seeded into 6-well plates containing 25 mm coverslips (around 4×10^5 mixed cells per coverslip) in the following combinations: winner+winner, winner+loser, and loser+loser. To evaluate the role of specific Flower protein domains in cell competition, three additional constructs were generated, each encoding a truncated version of Flower fused to mScarlet I-TM, targeting either the N-terminus, Exon 3, or C-terminus. These constructs were individually transfected into Flower KO astrocytes and co-cultured with an equal number of Flower KO astrocytes expressing the lose isoform. After 24 h of co-culture, cells were fixed in 4% PFA for 10 min at RT. DAPI was added prior to fixation to label late apoptotic cells. Immunocytochemistry was performed using an antibody against CC3 to detect early apoptotic cells.

For peptide-based assays, synthetic peptides corresponding to the N-terminus, Exon 3, and C-terminus regions of Flower were added to astrocyte cultures at a concentration of 1 µg/ml. Astrocytes expressing either win or lose isoforms were treated for 24 h prior to fixation and analysis. Finally, Live or fixed cells were imaged using a confocal microscope (LSM780, Zeiss) equipped with a 40×/1.3 NA objective. Cell counts and cell death analysis were performed manually using Fiji (ImageJ).

To evaluate the role of secreted Flower in cell fitness, supernatants from T-75 flasks were collected, and EVs were isolated by ultracentrifugation (see EV isolation). Approximately 20 µg of protein from the pelleted supernatant can be obtained from one flask (10 ml). Ten micrograms of pelleted EVs were applied to approximately 1×10^5 unfit astrocytes expressing mFwe1-mCherry, which were seeded on a 12.5 mm coverslip for the fitness assay. After 24 h, cells were fixed and stained for CC3 to quantify apoptotic cells.

Amyloid Beta1–42 protofibril generation and application

Synthetic $A\beta_{1\text{-}42}$ peptides labeled with HiLyte Fluor 647 (Anaspec Inc.) were dissolved in 1% NH_4OH and subsequently diluted in 1x PBS to a final concentration of 100 µM. The solution was incubated at 37 °C for 4 h to allow for protofibril formation. Protofibrils were then diluted to a final concentration of

0.1 μM and applied to cortical neuron cultures on DIV 7 for 6 days to assess cytotoxicity. WT cortical neuron cultures were transduced with lentiviruses encoding mFwe2–mScarlet I, mFwe C-terminal–mScarlet I, or cytosolic mScarlet I at DIV 1. Cells were then either fixed and immunostained for apoptosis analysis or collected for flow cytometry to assess $A\beta_{1-42}$ protofibril uptake.

Plasmid cloning

Plasmids encoding mouse Fwe1, Fwe2, Fwe3, and Fwe4, as well as human Fwe3 and Fwe4 with C-terminal mTFP tags, were generated in a previous study[5]. To generate constructs with a C-terminal mCherry tag, the mCherry sequence was subcloned into the original pMax-Flower-mTFP plasmids by replacing the mTFP tag using the restriction enzymes XbaI and XhoI. To construct plasmids encoding truncated Flower fusion proteins with a TM domain, the pDisplay-pHuji vector (#61556, Addgene), which contains the PDGFR TM domain, was used as the source. The mScarlet I sequence and the PDGFR TM domain were subcloned into the pMax backbone to generate the pMax-mScarlet I-TM construct. Truncated Flower sequences were PCR-amplified using gene-specific primers. For the N-terminal region of Flower, amplification was performed using the forward primer 5′-ATGTATAGGAAGATCTATGAGCGGCTCGGGCGCCGCC-3′ and the reverse primer 5′-ATGTATACGCGGATCCCGCCAGGCGGCACAGCCAGCG-3′. For Exon3, the forward primer was 5′-ATGTATAGGAAGATCTATCATGAATGCCTTCATCTTG-3′, and the reverse primer was 5′-ATGTATACGCGGATCCCCCGCAGTAGAAGACAGCCTT-3′. The C-terminal Flower sequence, flanked by BglII and BamHI restriction sites, was synthesized by BioCAT in the pBluescript II SK(+) vector. These truncated sequences were subcloned into the pMax-mScarlet I-TM plasmid to generate pMax-truncated-Fwe-mScarlet I-TM constructs. To generate tagged versions of Fwe1 and Fwe2, synthetic sequences encoding a 3×Flag tag (with ClaI and EcoRI sites) or a 3×HA tag (with XbaI and XhoI sites) were obtained from BioCAT and cloned into the pMax-mScarletI-mFwe1-mTFP or pMax-mScarletI-mFwe2-mTFP plasmids, respectively. The 3×Flag sequence replaced mScarlet I, and the 3×HA sequence replaced mTFP, resulting in the final constructs: pMax-3×Flag-mFwe1-3×HA and pMax-3×Flag-mFwe2-3×HA. For the generation of pMax-mFwe1-pHluorin2 and pMax-mFwe2-pHluorin2 plasmids, the C-terminal pHluorin2 sequence was PCR-amplified using the forward primer 5′-TGCTCTAGAATGTCAAAGGGCGAGGAG-3′ (XbaI site) and the reverse primer 5′-CCGCTCGAGTTATTTGTACAACTCGTC-3′ (XhoI site). The parental plasmids pMax-mFwe1-mTFP and pMax-mFwe2-mTFP were digested with XbaI and XhoI to remove the mTFP tag, and the amplified pHluorin2 fragment was inserted using T4 DNA ligase. To construct N-terminal pHluorin2 fusions (pMax-pHluorin2-mFwe1 and pMax-pHluorin2-mFwe2), pHluorin2 was PCR-amplified using the forward primer 5′-CCGGAATTCATGTCAAAGGGCGAGGAG-3′ (EcoRI site) and the reverse primer 5′-GCTAGCGCTACCGCCGCTTCCGCCGCTCCCACCCTCGAGTTTGTACAACTCGTC-3′ (NheI site). The pMax-Halo-mFwe1 and pMax-Halo-mFwe2 plasmids were digested with EcoRI and NheI to remove the Halo tag, which was replaced by the PCR-amplified pHluorin2 sequence. The lentiviral expression vector pCDH-EF1 (#72266, Addgene) was used to generate pCDH-mFwe2-mScarletI. The mFwe2 coding sequence was cloned into the pCDH-EF1 plasmid using EcoRI and

XbaI, and mScarlet I was inserted using the forward primer 5′-ATGTATATGCTCTAGAATGGTGAGCAAGGGCGAG-3′ and reverse primer 5′-ATGTATACCCCCCGGGTTACTTGTACAGCTCGTCCAT-3′. To generate pCDH-mFwe C ter.-mScarlet I, the C-terminal region of Flower was PCR-amplified using the forward primer 5′-CCGGAATTCATGCTGGAGGGGGAGCTG-3′ (EcoRI site) and the reverse primer 5′-CTAGCTAGCCTTGCCATCCGCGAT-3′ (XbaI site), and used to replace the mFwe2 sequence in the pCDH-mFwe2-mScarlet I backbone. All constructs were verified by Sanger sequencing using gene-specific forward and reverse primers (Microsynth Seqlab).

Surface plasmon resonance binding analysis

Series Sensor Chips CM5 were obtained from Cytiva (Freiburg, Germany). Amine coupling reagents N-(3-dimethylaminopropyl)-N'-ethylcarbodiimide hydrochloride (EDC) and N-hydroxysuccinimide (NHS), along with ethanolamine hydrochloride, were purchased from Merck KGaA (Darmstadt, Germany). HEPES buffer, NaCl, and NaOH were sourced from Carl Roth (Karlsruhe, Germany), Grüssing GmbH (Filsum, Germany), and VWR Chemicals (Darmstadt, Germany), respectively. TWEEN 20 and dimethyl sulfoxide (DMSO) were acquired from Sigma-Aldrich (Steinheim, Germany) and Thermo Fisher Scientific (Dreieich, Germany). For SPR analysis, HBS-P (0.01 M HEPES, 0.15 M NaCl, 0.05% TWEEN 20) served as running buffer during surface preparation. All glassware was rinsed with 50 mM NaOH and Milli-Q water before use. Ligand 1562II was immobilized onto a CM5 sensor chip via amine coupling using a BIACORE T200 system (Cytiva, Freiburg, Germany). Carboxyl groups were activated with a 1:1 mixture of 391.2 mM EDC and 100 mM NHS (10 µl/min, 7 min). 1562II (200 µg/ml in 10 mM HEPES, pH 5.5) was injected for 2 min (10 µl/min), achieving an immobilization level of about 4690 RU. Residual esters were blocked with 1 M ethanolamine-HCl (pH 8.5, 7 min). A reference surface was prepared by activation and immediate deactivation without ligand.

Binding of 1825 and 1826 to immobilized 1562II was assessed at 25 °C using HBS-P with 3 % DMSO as running buffer. Solvent correction was performed using DMSO dilutions (2.5 - 3.8 %). Analytes were prepared at 15, 30, and 40 µM in running buffer and injected in triplicate. Each cycle included a 180 s association and 300 s dissociation phase at 30 µl/min. Surfaces were washed with running buffer and cleaned with 50 % DMSO. Regeneration was achieved using 5 M NaCl followed by deionized water. Data were processed with BIACORE T200 Evaluation Software v3.2.1, applying double referencing and solvent correction prior to curve fitting.

Harvest of secreted Flower fractions and extracellular vesicles

WT astrocytes cultured for 9–12 days were electroporated with constructs expressing mFwe2-pHluorin2, 3×Flag-mFwe1-3×HA, or 3×Flag-mFwe2-3×HA. Following electroporation, 4×10^6 cells were cultured in a T-75 flask containing 10 ml of culture medium for 2–3 days. The medium was supplemented with 10% exosome-depleted FCS, prepared by ultracentrifuging heat-inactivated FCS (Gibco) at 100,000 × g for 16 h at 4 °C to remove serum-derived EVs. To harvest astrocyte-derived

EVs, conditioned medium was collected and centrifuged at 300 × g for 10 minutes to remove cell debris. The supernatant was then filtered through a 0.22 µm syringe filter (Millipore) to eliminate residual debris and large vesicles. Sequential ultracentrifugation was performed: first at 10,000 × g for 40 minutes at 4 °C to remove apoptotic bodies, followed by 100,000 × g for 1 h and 15 minutes at 4 °C to pellet secreted Flower-containing fractions and EVs. All ultracentrifugation steps were carried out using Ultra-Clear centrifuge tubes (Beckman Coulter) in an Optima XPN-80 ultracentrifuge (Beckman Coulter). For analysis of secreted Flower and EV content, pellets were resuspended in D-PBS and applied to 12.5 mm coverslips pre-coated with poly-L-ornithine in a 24-well plate. After a 1 h incubation at 37 °C, coverslips were centrifuged at 1,000 × g for 10 min to allow EVs to settle. The supernatant was then carefully removed, and the samples were fixed with 4% PFA for 20 min, followed by immunostaining.

Western blot analysis

Cells were lysed on ice using a buffer containing 50 mM Tris-HCl (pH 7.4), 1 mM EDTA, 250 µM PMSF, 1% Triton X-100, 150 mM NaCl, 1 mM DTT, 1 mM sodium deoxycholate, and a protease inhibitor cocktail (Roche). Cell lysis was facilitated by mechanical scraping, followed by incubation on ice for 30 min. Lysates were centrifuged at 16,000 × g for 10 min at 4 °C, and the supernatants were collected for subsequent analysis. Protein concentrations were determined using the Pierce 660 nm Protein Assay (Thermo Fisher Scientific) according to the manufacturer's instructions.

Equal amounts of protein (30 µg per lane for cell lysates, 10 µg per lane for secreted Flower fractions from conditional medium) were resolved by SDS–PAGE using NuPAGE precast gels (Invitrogen) and transferred onto nitrocellulose membranes. Membranes were blocked for 30 min at RT in TBS-T buffer (20 mM Tris-HCl, 150 mM NaCl, 0.05% Tween-20, pH 7.4) containing 5% (w/v) non-fat dry milk. Membranes were then incubated with primary antibodies overnight at 4 °C. After washing three times in TBS-T, membranes were incubated with HRP-conjugated secondary antibodies for 45 min at RT. Signal detection was performed using enhanced chemiluminescence reagents (SuperSignal West Dura Chemiluminescent Substrate, Thermo Fisher Scientific), and images were acquired using the FluorChem E documentation system (BioLabTec GbR).

Immunofluorescence

Cells grown on coverslips were fixed in 4% PFA for 10 min at RT and subsequently washed three times with D-PBS. Permeabilization was performed in D-PBS containing 0.1% Triton X-100 (Roth) for 10 min. Samples were then incubated in blocking buffer (D-PBS supplemented with 2% BSA) for 30 min to reduce non-specific binding. Primary antibodies were diluted in blocking buffer and applied for 1 h at room temperature. Following three washes with D-PBS, samples were incubated with the appropriate Alexa Fluor-conjugated secondary antibodies for 45 min at RT in the dark. After three additional washes with D-PBS, samples were counterstained with or without DAPI (1:1000) and mounted using Fluoromount-G Mounting Medium (Invitrogen). Cell death was analyzed using CC3

and DAPI markers by confocal microscopy with a 40×/1.3 NA objective. Secreted Flower particles were analyzed by super-resolution SIM using a 63×/1.4 NA objective. SIM imaging were performed on a Zeiss Elyra PS.1 microscopic SIM System with Zen 2010 software for device control and high-resolution image processing. Images were acquired as z-stacks with 0.2-µm intervals through the entire cell. Single-plane and maximum intensity projections were used to illustrate vesicle co-localization.

Amyloid plaques extraction by laser capture dissection

Freshly isolated brains from APP transgenic mice were fixed in 4% PFA overnight and subsequently processed for paraffin embedding. Fixed tissues were dehydrated through a graded ethanol series (70%, 80%, and 95% ethanol for 1.5 h each), followed by three washes in 100% ethanol (2 h each). Samples were cleared in xylene (three times for 1.5 h) to remove residual ethanol, then infiltrated with paraffin wax at 60 °C (two rounds, 1.5 h each). Embedded tissues were oriented in molds and cooled at RT to solidify.

Paraffin blocks were sectioned at 5 µm thickness using a microtome. Sections were floated on a 63–65 °C water bath to remove wrinkles, then mounted onto RNAse-free PEN membrane-coated glass slides (VWR, Cat. No. 76414-898) for laser microdissection (Leica). Slides were air-dried and stained with Congo Red to label amyloid plaques and Hematoxylin to visualize cellular architecture prior to RNA extraction.

RNA isolation, cDNA synthesis and RT–qPCR

Total RNA from cultured cells was extracted using TRIzol reagent (Thermo Fisher Scientific) according to the manufacturer's protocol. Briefly, 5 × 10 cells were homogenized in 500 µl TRIzol, followed by the addition of 100 µl chloroform. Samples were centrifuged at 12,000 × g for 15 min at 4 °C, and the aqueous phase containing RNA was transferred to a fresh tube. RNA was precipitated with an equal volume of 100% isopropanol, washed once with 75% ethanol, air-dried, and dissolved in DEPC-treated H_2O.

RNA from microdissected samples was extracted using the RNeasy FFPE Kit (QIAGEN) following the manufacturer's instructions. Briefly, microdissected tissues were lysed in PKD buffer, followed by treatment with Proteinase K. Lysates were incubated at 56 °C for 15 min, then at 80 °C for 15 min, and placed on ice for 3 min. Samples were centrifuged at 20,000 × g for 15 min, and the supernatant was treated with DNase I for 15 min at RT. RNA was precipitated by the addition of RBC buffer and ethanol, bound to an RNeasy MinElute spin column, washed, and eluted in RNase-free water. RNA quantity and purity were assessed using a NanoDrop spectrophotometer.

For cDNA synthesis, 1 µg of total RNA was reverse-transcribed using the ABScript II cDNA First-Strand Synthesis Kit (ABclonal) according to the manufacturer's instructions. The reaction mix contained Random Primer Mix, 10 mM dNTPs, and ABScript II reverse transcriptase. Reactions were incubated at 25 °C for 5 min, followed by 42 °C for 1 h, and terminated at 80 °C for 5 min. Real-time quantitative PCR (RT–qPCR) was performed using Genious 2× SYBR Green Fast qPCR Mix

(ABclonal) on a CFX96 Touch Real-Time PCR Detection System (Bio-Rad). Each reaction contained 10 ng of cDNA and gene-specific primers targeting mFwe1, mFwe2, mFwe3, mFwe4, Caspase3, Bax, and Bcl2. GAPDH served as the internal control. Gene expression was normalized to GAPDH using the ΔCt method, and relative expression was calculated by the ΔΔCt method.

Flower topology experiments

To investigate the membrane topology of the Flower protein, mFwe1 and mFwe2 fusion constructs were generated by incorporating the ratiometric pH-sensitive fluorophore pHluorin2. The pHluorin2 tag was fused to either the N- or C-terminus of the Flower protein. Additionally, syb2-pHluorin2 and cytosolic pHluorin2 constructs were used as internal controls. WT astrocytes were transfected individually with each pHluorin2 construct. Following transfection, cells were plated onto glass coverslips and allowed to adhere for 24 h. Fluorescence measurements were acquired using a confocal microscope (LSM 780, Zeiss) equipped with a 40× objective. Images were recorded in 0.5 Hz. Fluorescence was monitored before and after perfusion with 200 µM carbonyl cyanide m-chlorophenyl hydrazone (CCCP, Sigma), using excitation wavelengths of 405 nm and 488 nm. CCCP induces cytosolic acidification, which alters the fluorescent properties of pHluorin2. In acidic conditions, pHluorin2 exhibits a decrease in excitation at 395 nm and an increase at 475 nm.

Statistics and reproducibility

Data were analyzed using SigmaPlot version 14.5. The specific statistical tests used are indicated in each figure legend. Student's t-test and Tukey's test were applied to assess statistically significant differences between groups, as appropriate. All values are presented as mean ± SEM from independent experiments.

Figure Legend

Figure 1. Flower is highly expressed in a subset of astrocytes near amyloid plaques in the neocortex.

a, RT-qPCR analysis of mouse Flower splice variant expression in plaque versus non-plaque areas of APP mouse cortices. Left: Representative image of a cortical slice from an APP mouse stained with Congo Red to label amyloid plaques (red) and hematoxylin to stain cell nuclei (blue). Plaque areas (red circles) were isolated for RT-qPCR, with non-plaque areas (black circles) serving as controls. Right: RT-qPCR quantification of fold changes in Flower expression between plaque and non-plaque areas, normalized to the housekeeping gene GAPDH (N=2). **b,** RT-qPCR analysis of Flower expression in cortices of APP mice compared to WT controls (N=2). **c,** Schematic representation of mouse Flower isoforms (mFwe1–4), illustrating comparable exon and intron structures across splice variants. **d–f,** Representative confocal images of the neocortex from APP mice. Amyloid plaques were labeled with Thioflavin-S (Thio-S) (cyan), and glial cells were stained with anti-GFAP (astrocytes) and anti-IBA1 (microglia). Scale bar: 50 µm. **e-f,** Endogenous Flower was stained with anti-Flower antibody #1557 (magenta) along with glial markers (yellow). **g,** Quantification of Flower-high-expressing astrocytes and microglia in plaque-associated regions compared to non-plaque areas, based on the total counted glial cells. Left: astrocytes; right: microglia, derived from images in **e** and **f** (N=3 mice; n=30 images; 1167 astrocytes and 967 microglia were analyzed). White arrows indicate Flower-expressing astrocytes near plaques. **h,** Histological staining of post-mortem brain cortex from AD patients. Plaques are marked with black circles. Left: astrocytes stained with anti-GFAP antibody. Right: co-staining for Flower (blue) and astrocytes (brown). Black arrows indicate double-positive cells. Scale bar: 50 µm. **i,** Confocal images of post-mortem brain cortex from AD patients. Flower (yellow) and GFAP (cyan) were stained to label Flower-expressing astrocytes. White arrows point to Flower-expressing astrocytes near plaques. **j,** Quantification of Flower-high-expressing astrocyte populations near plaques versus non-plaque areas from (**g**) (N=3 donor; n=45 images; n=1096 cells). Data are presented as mean ± SEM. Statistical significance was determined using Student's t-test: *$p < 0.05$, ***$p < 0.001$.

Figure 2. Flower-mediated regulation of cell fitness in primary astrocytes. a, Schematic of the experimental procedure. Primary astrocytes were isolated from Flower KO pups and cultured for 9–12 days before electroporation. Individual Flower isoforms were introduced into astrocytes via electroporation using a single cuvette. Transfected cells were then mixed at a 1:1 ratio to establish homotypic and heterotypic co-cultures. After 24 h of co-culture in a 6-well plate, cells were fixed and stained for cell death markers. Confocal imaging was used to assess cell death resulting from Flower-mediated cell selection. **b,** Confocal images of primary astrocytes expressing the "win" Flower isoform (yellow) co-cultured with astrocytes expressing the "lose" isoform (cyan). Cell-cell contacts between isoform-expressing cells were analyzed after 24 h. Cultures were fixed and stained with cleaved caspase-3 (CC-3; magenta) to mark apoptotic cells, while DAPI staining (blue), applied before fixation, identified non-intact cells or fragmented nuclei indicative of late apoptosis. Scale bar, 20 µm. White

arrows indicate CC3+ apoptotic cells, and green arrows point to fragmented DAPI+ nuclei. **c,** Quantification of cell death in pairwise win-win, lose-lose, and win-lose co-cultures. Cell death was assessed based on CC-3 and DAPI staining (n= 500-1200 cell contacts; N=3 independent mouse preparations). **d,** Quantification of cell death in individual isoform-expressing cells in heterotypic win-lose pairwise co-cultures (n= 260-360 cell contacts; N=2 independent mouse preparations). Data are presented as mean ± SEM. Statistical significance was determined using Student's t-test: *p < 0.05, **p < 0.01, ***p < 0.001.

Figure 3. N- and C-termini of Flower proteins are localized on the intracellular side of mouse primary astrocytes. a-f, WT astrocytes were transfected with pH-sensitive pHluorin2 constructs to evaluate the orientation of the N- and C-termini of Flower proteins (mFwe1 and mFwe2) in relation to the vesicle lumen or cytoplasm. Cytosolic-pHluorin2 and Syb2-pHluorin2 were used as internal controls, representing known pHluorin2 localization in the cytoplasm and vesicle lumen, respectively. Ionophore CCCP was applied to transfected cells to induce pH changes, while DMSO served as the control vehicle. Live-cell confocal imaging was used to record ratiometric changes by sequential excitation at 405 nm and 488 nm. Construct details and sample sizes are as follows: cytosolic-pHluorin2 (DMSO, n = 19 cells; CCCP, n = 32 cells), mFwe1-pHluorin2 (DMSO, n = 34; CCCP, n = 57), pHluorin2-mFwe1 (DMSO, n = 29; CCCP, n = 31), Syb2-pHluorin2 (DMSO, n = 50; CCCP, n = 54), mFwe2-pHluorin2 (DMSO, n = 37; CCCP, n = 71), and pHluorin2-mFwe2 (DMSO, n = 42; CCCP, n = 60). N = 3 independent experiments. **g,** Confocal image of WT astrocytes lentivirally infected with mFwe2–mScarlet I (red). Cells were counterstained with DAPI to label cell nuclei (blue). Scale bar, 20 µm.

Figure 4. Secreted Flower win isoform facilitates cellular fitness through extracellular vesicles. a, Confocal images of cortical brain slices from APP-transgenic mice and postmortem human brain tissue from AD patients. Win Flower isoforms were detected using a C-terminal-specific Flower antibody (#C-1557). Arrows indicate Flower signal localized in the extracellular matrix. A white dashed circle marks a plaque in the human tissue. Scale bar, 20 µm. **b,** SIM images of supernatant fractions collected from WT or mFwe2-pHluorin2–expressing astrocyte cultures. Pelleted fractions were deposited onto polyornithine-coated glass coverslips, fixed, and stained with a polyclonal Pan-Flower antibody recognizing both N- and C-termini, along with DiD to label lipids. In mFwe2-overexpressing cultures, anti-GFP was used to detect overexpressed Flower. Scale bar, 1 µm. **c,** Quantification of the co-localization between Flower-positive particles and the lipid dye DiD from (**b**). **d,** Schematic of transfected Flower constructs (Fwe2 “win” and Fwe1 “lose”) used to analyze secreted Flower in astrocyte supernatants. **e,** SIM images of Flower fragments isolated from the supernatant of WT astrocytes overexpressing Fwe constructs. Pelleted supernatant were fixed and stained with anti-Flag (cyan), anti-HA (yellow), and DiD (magenta) to visualize N- and C-terminal fragments and their association with extracellular vesicles. Scale bar, 1 µm. **f,** Western blot analysis of secreted mFwe1 and mFwe2 from Fwe constrcuts transfected WT astrocyte culture. Ten micrograms of EV protein

were loaded per lane. Blots were first probed with anti-Flag antibody, then stripped and sequentially reprobed with anti-HA and anti-Pan-Flower antibodies. **g,** Quantification of relative secreted protein amount of Fwe2 compared to Fwe1 from (**f**) (N = 3 independent experiments). **h,** Schematic of the experimental workflow for assessing the effect of secreted Flower EVs on cellular fitness. Astrocytes were cultured for two weeks following cortical isolation. Supernatants were collected, and suspended fractions were pelleted via ultracentrifugation. Enriched Flower-containing EVs were analyzed (**e–g**) and applied to unfit cell populations to evaluate their role in inducing cell death. **i,** Confocal images of mFwe1-expressing unfit cells treated with Flower fragments derived from WT, mFwe1-, or mFwe2-overexpressing astrocyte cultures. Approximately 10 µg of EVs were applied to 100,000 recipient cells seeded on a 12.5 mm coverslip in a 24-well plate. After 24 h, cells were fixed and stained with anti-CC3 to label apoptotic cells. Cell death was defined by positive CC3 staining. Scale bar, 50 µm. **j,** Quantification of apoptotic cells from (**i**) (control n = 616; WT EVs n = 665; mFwe1 EVs n = 687; mFwe2 EVs n = 917; N = 3). Data are mean ± SEM. Statistical significance: one-way ANOVA with Tukey's post hoc test, *p < 0.001.

Figure 5. N terminus of Flower induces unfit cells apoptosis while C terminus of Flower impedes unfit cells death. a, Schematic representation of putative signaling domains located at the N-terminus, C-terminus, and Exon 3 region of the full-length mFwe2 sequence. **b-j,** Cell fitness assays were performed using Flower KO astrocytes expressing the indicated Flower isoforms to generate fit or unfit cell populations. Cells were treated with specific signal peptides or co-overexpressed truncated Flower constructs for cell death rescue experiments. Cultures were fixed 24 h after treatment or co-culture, and cell death was assessed based on DAPI staining or CC3+ immunostaining. **b,** Confocal images of cells expressing specific Flower signaling domains (yellow) co-cultured with unfit mFwe1-mTFP-expressing “lose” cell populations (cyan). Cultures were stained with DAPI before fixation and anti-CC3 antibody (magenta) after fixation to analyze positively stained dead cells. Scale bar, 20 µm. **c,** Quantification of overall cell viability in co-cultures of Flower KO astrocytes expressing individual signaling domains (N terminus, exon3 or C terminus) with either fit (mFwe2) or unfit (mFwe1) cell populations (n = 255–342 cells per group; N = 3 independent experiments). Statistical significance was determined by two-way ANOVA with Holm-Sidak correction: ***p < 0.001. **d,** Detailed analysis of cell death in co-cultures of KO astrocytes expressing the N-terminal Flower construct (Flower N-term-TM) and mFwe1-expressing unfit cells, as shown in the first group of panel **c** (n = 307 cells; N = 3 independent experiments). **e,** Confocal images of synthetic Flower N-terminus peptides applied to mFwe1-expressing unfit cells. Cultures were fixed and stained as described. Control cells were treated with DMSO. Scale bar, 50 µm. **f,** Synthetic Flower signal peptides affect cell fitness. Peptides representing four Flower domains were incubated with mFwe1- or mFwe2-expressing cells for 24 h, and cell death was quantified. Data represent >300 cells per condition from N = 3 independent experiments. Statistical significance was determined by one-way ANOVA followed by Tukey’s post hoc test (**p < 0.01, *p < 0.001). **g,** Dose-dependent effect of the Flower N-terminal peptide on apoptosis in unfit cells. mFwe1- and mFwe3-expressing cells were treated with 0.1, 1, or 10 µg of N-terminal peptide or DMSO control for 24 h. Cell death was

quantified (n = 311–631 cells per condition; N = 3 independent experiments). Statistical significance was determined by one-way ANOVA with Tukey's post hoc test ($p < 0.05$, $p < 0.01$, $p < 0.001$). **h-i,** Role of the Flower C-terminus peptide in rescuing cell death induced by the N-terminus peptide. mFwe1- and mFwe3-expressing unfit cells were treated with suspended Flower N-terminus peptide and transfected with or without the C terminus-TM construct. **h,** Representative confocal images of the experiment, with DMSO-treated groups serving as controls. Scale bar, 50 µm. **i,** Quantification of dead cells following N-terminal peptide treatment, with or without co-expression of the C-terminal domain. mFwe1- and mFwe3-expressing cells were treated for 24 h, and cell death was quantified (n = 278–617 cells per condition; N = 3 independent experiments). Statistical significance was assessed by one-way ANOVA with Tukey's post hoc test ($p < 0.05$, $^{**}p < 0.001$). **j,** Quantitative RT-PCR analysis of Flower signal peptide-mediated cell death. KO astrocytes were transfected with mFwe1 to generate unfit cells and treated with the N-terminus peptide, with or without rescue by overexpression of Flower C- or N-terminus constructs. Apoptosis-related genes (Caspase-3, Bax, and Bcl2) were analyzed after 24 h (N = 3). Data are presented as mean ± SEM. Statistical significance was determined using Student's t-test: $^{*}p < 0.05$, $^{**}p < 0.01$, $^{***}p < 0.001$.

Figure 6. Astrocytes expressing the Flower win isoform restore neuronal survival following Aβ protofibril-induced death. a, Confocal images of transfected neuronal cultures treated with Aβ protofibrils–Alexa647. Wild-type (WT) neuronal cultures were lentivirally infected at DIV1 with Flower–mScarlet I constructs (mFwe2–mScarlet I or C-terminal–mScarlet I) or a control mScarlet I vector (yellow). At DIV7, cultures were treated with or without Aβ protofibrils–Alexa647 (cyan). Neuronal cultures were fixed after 6 days and stained with CC3 antibody (magenta) to identify apoptotic cells. Scale bar, 50 µm. Right: schematic representation of the corresponding cultures and treatments shown on the left. **b,** Quantification of CC3+ cell death from panel **a**. **c-d,** FACS analysis of Aβ protofibril uptake by glial populations. Neuronal cultures were trypsinized to evaluate the proportion of Aβ-positive cells. Untreated cells (black), WT group (white), mFwe2-expressing cells (red), and C-terminus-expressing cells (magenta) were analyzed (N = 3). **d,** Quantification of Aβ-positive cell populations from panel **c. e-f,** Analysis of Aβ aggregate size in vector-transfected control (WT), mFwe2-expressing, and C-terminus-expressing cultures after 6 days. **f,** Size distribution of Aβ aggregates in the three culture conditions (N = 3). Data are presented as mean ± SEM. Statistical significance was determined using Student's t-test: $^{*}p < 0.05$, $^{**}p < 0.01$, $^{***}p < 0.001$.

Figure 7. Proposed model of Flower-mediated fitness regulation via secreted EV signaling.

The N- and C-terminal domains of Flower exert opposing effects on cellular fitness: the N-terminus promotes apoptosis, while the C-terminus supports cell survival. Astrocytes expressing the win isoform of Flower secrete high levels of Flower protein in the form of membrane-associated EVs and/or non-membranous fragments, potentially generated through proteolytic cleavage. Flower may localize directly to intracellular vesicles or be packaged into larger vesicular structures prior to release. The precise identity and composition of these Flower-positive vesicles remain undefined. Secreted

Flower exists in both full-length forms (with attached N- and C-termini) and cleaved fragments containing only one terminal domain. The N-terminal domain activates a Bax- and cleaved caspase-3-dependent apoptotic pathway in recipient ‘loser’ cells, leading to their elimination. Conversely, overexpression of the C-terminal domain, anchored to the plasma membrane (Fwe C-TM), in recipient ‘loser’ cells neutralizes this pro-apoptotic signal by directly binding the N-terminal region. Thus, the C-terminus provides intrinsic cellular protection by antagonizing the death-promoting activity of the N-terminus.

Additional information

Extended Data Table 1. Plasmids used in this study

Plasmids
pMax-mFwe1-mTFP
pMax-mFwe2-mTFP
pMax-mFwe3-mTFP
pMax-mFwe4-mTFP
pMax-mFwe1-Cherry
pMax-mRFP-mFwe2
pMax-mFwe3-Cherry
pMax-mFwe4-Cherry
pMax-hFwe3-mTFP
pMax-hFwe4-mTFP
pMax-hFwe3-mCherry
pMax-hFwe4-mCherry
pMax-HA-mFwe N ter.-mScarlet I-TM
pMax-HA-mFwe Exon3-mScarlet I-TM
pMax-HA-mFwe C ter.-mScarlet I-TM
pMax-pHluorin2
pMax-Syb2-pHluorin2
pMax-mFwe1-pHluorin2
pMax-mFwe2-pHluorin2
pMax-pHluorin2-mFwe1
pMax-pHluorin2-mFwe2
pMax-3xFlag-mFwe1-3xHA
pMax-3xFlag-mFwe2-3xHA
pMax-3xFlag-mFwe3-3xHA
pMax-3xFlag-mFwe4-3xHA
pCDH-mFwe2-mScarlet I

pCDH-mFwe C ter.-mScarlet I
pMDL g/p
pRSV-Rev
pMD2.G

Extended Data Table 2. Antibodies used in this study

Antibody anti-	Supplier	Identifier	Source	Dilution	application
Pan-Flower	Generated in house	Polyclonal, raised against full length protein	rabbit	1:100 1:1000	ICC WB
Flower (#1557)	Generated in house	Polyclonal, sequence-directed (targeted to C-terminal)	rabbit	1:200	IHC
HA	Roche	11867423001 Clone 3F10	rat	1:100 1:1000	ICC WB
Flag	Sigma-Aldrich	F1804 Clone M2	mouse	1:100 1:1000	ICC WB
RFP (DsRed)	GenWay/aviva systems	OARA01891	rabbit	1:200	ICC
Cleaved Caspase-3	Cell signaling	#9661	rabbit	1:500	ICC
Iba1	FujiFilm	019-19741	rabbit	1:500 1:200	ICC IHC
Iba1	Novus Biologicals	NB100-1028	goat	1:200	IHC
GFAP	Abcam	ab4674	chicken	1:1000	ICC IHC
GFAP	DAKO, Agilent Technologies	Z0334	rabbit	1:500	IHC
GFP	Abcam	ab13970	chicken	1:1000	ICC
Anti-Rabbit IgG (H+L)-Alexa Fluor488	Jackson ImmunoResearch Europe Ltd	AB_2338046	goat	1:1000	IHC

Anti-Rabbit IgG (H+L)-Cy3	Jackson ImmunoResearch Europe Ltd	AB_2338240	goat	1:1000	IHC
Anti-mouse IgG (H+L)-Alexa Fluor488	Invitrogen	A11001	goat	1:1000	ICC
Anti-mouse IgG (H+L)-Alexa Fluor647	Invitrogen	A21235	goat	1:1000	ICC
Anti-chicken IgY (H+L)-Alexa Fluor488	Invitrogen	A11039	goat	1:1000	IHC
Anti-chicken IgY (H+L)-Alexa Fluor568	Invitrogen	A11041	goat	1:1000	IHC
Anti-rabbit IgG (H+L)-Alexa Fluor568	Invitrogen	A11011	goat	1:1000	ICC
Anti-rabbit IgG (H+L)-Alexa Fluor647	Invitrogen	A21244	goat	1:1000 1:1000	ICC IHC
Anti-rat IgG (H+L)-Alexa Fluor488	Invitrogen	A11006	goat	1:1000	ICC
Anti-rat IgG (H+L)-Alexa Fluor568	Invitrogen	A11077	goat	1:1000	ICC
Anti-goat IgG (H+L)-Alexa Fluor647	Invitrogen	A21447	donkey	1:1000	IHC
Anti-mouse IgG (H+L)-HRP	Invitrogen	32430	goat	1:1000	WB
Anti-rabbit IgG (H+L)-HRP	EMD Millipore	AP307P	goat	1:5000	WB
Anti-Rat IgG (H+L)-HRP	GE healthcare	NA935	goat	1:5000	WB

Extended Data Table 3. Synthetic peptides used in this study

Peptide name	Supplier	aa sequence	application
#1824 Fwe Exon3	Generate in house	FCCQFVEFANTVAEKVDRLRRSWQKAVFYC	Cell culture
#1825 Fwe N ter.	Generate in house	MSGSGAAGAAAGPAPPAQEEGMTWWYRWLCR	Cell culture, SPR
#1826 Fwe C ter.	Generate in house	GKKGDAISYARIQQQRQQADEEKLAETFEGEL	Cell culture, SPR
#1562II Fwe C ter. (Cys in N term)	Generate in house	c-GKKGDAISYARIQQQRQQADEEKLAE	SPR

		TFEGEL	
Fwe Exon3 (long)	Biozol/biomatik	Biotin-MNAFILLLCEAPFCCQFVEFANTVAEKVDRLRRSWQKAVFYC	Cell culture
Fwe Exon3 (short)	Biozol/biomatik	Biotin-FCCQFVEFANTVAEKVDRLRRSWQKAVF	Cell culture

Extended Data Table 4. RT–qPCR primers used in this study

Gene	Primer 5' – 3'	Size(bp)
mFwe1	Forward: ACTGACTCATCCAATAACAGG Reverse: ACCATGCCTACACATACATTAG	200
mFwe2	Forward: GCCATTTCTTATGCTCGGAT Reverse: GCCATTTAACAGAGCTGACA	173
mFwe3	Forward: GTCTTCTACTGCGGGCAT Reverse: AGAGGGAAATGGTGTTTCTG	82
mFwe4	Forward: TTGCTAAATCCTGGGTGTCC Reverse: TGTTCAGAGGGTGGATAGTG	99
Bax	Forward: CTACAGGGTTTCATCCAG Reverse: TATTGCTGTCCAGTTCATCT	142
Bcl2	Forward: TACCTGAACCGGCATCT Reverse: CAGCCAGGAGAAATCAAACA	108
Casp3	Forward: GGCTTGCCAGAAGATAC Reverse: CTCCAGGAATAGTAACCAG	75
GAPDH	Forward: GTATGTCGTGGAGTCTACTG Reverse: TATTTCTCGTGGTTCACACC	141

Extended Data Figure Legend

Extended Data Figure 1. Human Flower isoforms mediate cellular fitness in primary astrocytes. **a,** Confocal images of mouse primary Flower KO astrocytes expressing the human Flower "win" isoform 4 (yellow) co-cultured with astrocytes expressing the human "lose" isoform 3 (cyan). Cell-cell contacts between hFwe 3- and hFwe 4-expressing cells were analyzed after 24 h. Cultures were fixed and stained with CC-3 (magenta) to identify apoptotic cells. DAPI staining (blue), applied before fixation, marked non-intact cells or fragmented nuclei indicative of late apoptosis. Scale bar, 20 µm. **b,** Quantification of cell survival in co-cultures. Cell death were counted based on CC-3 and DAPI staining (N = 2 independent experiments). **c,** Quantification of cell death in win-lose co-culture from **b**.

Data are presented as mean ± SEM. Statistical significance was determined using Student's t-test: *p□<□0.05, **p□<□0.01, ***p□<□0.001.

Extended Data Figure 2. Cleaved Flower fragments in astrocytes and their secreted forms.

a–b, Western blot analysis showing proteolytic cleavage of overexpressed Flower isoforms. Flower KO astrocytes were transfected with 3×Flag-mFwe-3×HA constructs, containing a Flag tag at the N-terminus and an HA tag at the C-terminus. Lysates from untransfected Flower KO astrocytes served as negative controls. GAPDH was used as a loading control (N = 3 independent experiments). **a,** Left: Blot probed with anti-Flag antibody to detect N-terminal fragments from all expressed isoforms. Right: Quantification of full-length and cleaved fragments. **b,** Left: Blot probed with anti-HA antibody to detect C-terminal fragments. Right: Quantification of full-length and cleaved fragments. **c,** Longer exposure of a separate blot from the same experiment, reprobed with anti-Pan-Flower antibody to confirm band identity. **d,** Analysis of secreted Flower fragments from overexpressing astrocytes. Supernatants from Flower KO astrocyte cultures transduced with 3×Flag-Flower-3×HA constructs were analyzed by immunostaining with anti-Flag (N-terminal) and anti-HA (C-terminal) antibodies. Co-staining with a lipid dye assessed potential association with EVs. SIM was performed on supernatants from mFwe1- and mFwe2-expressing cells (N = 3; mFwe1: 5,330 particles; mFwe2: 5,348 particles). Data are presented as mean ± SEM. Statistical significance was determined by one-way ANOVA followed by Tukey's post hoc test (*p < 0.05, **p < 0.01).

Extended Data Figure 3. Flower 'win' isoform yields higher transfection efficiency than the 'lose' isoform in mouse astrocytes.

a, Primary mouse astrocytes were transfected with either the "lose" isoform (mFwe1–mCherry or mFwe1–mTFP) or the "win" isoform (mRFP–mFwe2 or mFwe2–mTFP) to assess transfection efficiency. The number of fluorescent mFwe1^{+} and mFwe2^{+} cells was quantified from confocal images of separately cultured populations. N□=□2 independent preparations; n□=□84 cells for mFwe1, n□=□101 cells for mFwe2. Statistical analysis was performed using Welch's t-test; two-tailed P□<□0.001 (**). **b,** Mean fluorescence intensity per cell from the same dataset as in (**a**), used to assess expression levels of mFwe1 and mFwe2. Red lines indicate median values. N□=□2 independent preparations; n□=□100 cells per group. Statistical comparison using the Mann–Whitney U test showed no significant difference.

Extended Data Figure 4. The N-terminal Flower domain does not induce cell death in fit cell populations. a, Schematic of constructs in which truncated Flower domains (N-terminus, Exon 3, or C-terminus) were fused to a transmembrane (TM) domain for plasma membrane (PM) localization. An HA tag was placed at the N-terminus and mScarlet-I at the C-terminus to assess membrane orientation. **b,** Confocal images of Flower KO astrocytes expressing truncated Flower domains

targeted to the PM. To verify surface expression, fixed, non-permeabilized cells were stained with anti-RFP–Alexa647 (magenta) and anti-HA (cyan). Scale bar, 50 μm. **c,** Confocal images of Flower KO astrocytes expressing specific truncated Flower domains (yellow) co-cultured with fit mFwe2–mTFP–expressing "win" cells (cyan). Cultures were stained with DAPI before fixation and with anti-cleaved caspase-3 (CC3; magenta) after fixation to detect apoptotic cells. Maximum intensity projection images are shown. Scale bar, 20 μm.

Extended Data Figure 5. Overexpression of the C-terminus Flower domain does not alter cell survival. a, Flower KO astrocytes were transfected with mFwe1 or mFwe3 to generate unfit cell populations. Co-transfection with the C-terminal Flower domain (C-term-TM) plasmid did not affect cell survival upon treatment with the control vehicle, DMSO. **b,** Quantitative RT-PCR analysis of apoptosis-related genes in transfected and treated cells. N = 3 independent experiments. Data are presented as mean ± SEM. Statistical significance was determined using Student's t-test: $p < 0.05$, $p < 0.01$, $p < 0.001$.

Extended Data Figure 6. SPR analysis showing interaction between the N- and C-terminal domains of Flower. SPR binding analysis showing interaction of Flower N-terminal and C-terminal peptides with immobilized Flower C-terminal peptide (engineered with an N-terminal cysteine for immobilization). Representative sensorgrams (left) and the corresponding quantification (right) demonstrate binding responses at increasing concentrations (15, 30, and 40 μM). Bar graph shows mean ± s.d. from three independent experiments.

References

1. Yao CK*, et al.* A synaptic vesicle-associated Ca2+ channel promotes endocytosis and couples exocytosis to endocytosis. *Cell* **138**, 947-960 (2009).

2. Xue L*, et al.* Voltage-dependent calcium channels at the plasma membrane, but not vesicular channels, couple exocytosis to endocytosis. *Cell Rep* **1**, 632-638 (2012).

3. Yao CK, Liu YT, Lee IC, Wang YT, Wu PY. A Ca2+ channel differentially regulates Clathrin-mediated and activity-dependent bulk endocytosis. *PLoS Biol* **15**, e2000931 (2017).

4. Chang HF*, et al.* Cytotoxic granule endocytosis depends on the Flower protein. *J Cell Biol* **217**, 667-683 (2018).

5. Ravichandran K*, et al.* Required minimal protein domain of flower for synaptobrevin2 endocytosis in cytotoxic T cells. *Cell Mol Life Sci* **82**, 8 (2024).

6. Brose N, Neher E. Flowers for synaptic endocytosis. *Cell* **138**, 836-837 (2009).

7. Kuo SP, Trussell LO. A new ion channel blooms at the synapse. *Neuron* **63**, 566-567 (2009).

8. Li TN, Chen YJ, Lu TY, Wang YT, Lin HC, Yao CK. A positive feedback loop between Flower and PI(4,5)P(2) at periactive zones controls bulk endocytosis in Drosophila. *Elife* **9**, (2020).

9. Seidenthal M*, et al.* Flower/FLWR-1 regulates neuronal activity via the plasma membrane Ca(2+) ATPase to promote recycling of synaptic vesicles. *Elife* **13**, (2025).

10. Merino MM, Rhiner C, Portela M, Moreno E. "Fitness fingerprints" mediate physiological culling of unwanted neurons in Drosophila. *Curr Biol* **23**, 1300-1309 (2013).

11. Rhiner C*, et al.* Flower forms an extracellular code that reveals the fitness of a cell to its neighbors in Drosophila. *Dev Cell* **18**, 985-998 (2010).

12. Merino MM, Levayer R, Moreno E. Survival of the Fittest: Essential Roles of Cell Competition in Development, Aging, and Cancer. *Trends Cell Biol* **26**, 776-788 (2016).

13. Merino MM, Rhiner C, Lopez-Gay JM, Buechel D, Hauert B, Moreno E. Elimination of unfit cells maintains tissue health and prolongs lifespan. *Cell* **160**, 461-476 (2015).

14. Madan E, Gogna R, Moreno E. Cell competition in development: information from flies and vertebrates. *Curr Opin Cell Biol* **55**, 150-157 (2018).

15. Marques-Reis M, Moreno E. Role of cell competition in ageing. *Dev Biol* **476**, 79-87 (2021).

16. Madan E*, et al.* Flower isoforms promote competitive growth in cancer. *Nature* **572**, 260-264 (2019).

17. Yekelchyk M*, et al.* Flower lose, a cell fitness marker, predicts COVID-19 prognosis. *EMBO Mol Med* **13**, e13714 (2021).

18. Costa-Rodrigues C, Couceiro J, Moreno E. Cell competition from development to neurodegeneration. *Dis Model Mech* **14**, (2021).

19. Coelho DS, Moreno E. Emerging links between cell competition and Alzheimer's disease. *J Cell Sci* **132**, (2019).

20. Gogna R, Shee K, Moreno E. Cell Competition During Growth and Regeneration. *Annu Rev Genet* **49**, 697-718 (2015).

21. Madan E*, et al.* Cell Competition Boosts Clonal Evolution and Hypoxic Selection in Cancer. *Trends Cell Biol* **30**, 967-978 (2020).

22. Parker T, Madan E, Gupta K, Moreno E, Gogna R. Cell Competition Spurs Selection of Aggressive Cancer Cells. *Trends Cancer* **6**, 732-736 (2020).

23. Dai DL, Li M, Lee EB. Human Alzheimer's disease reactive astrocytes exhibit a loss of homeostastic gene expression. *Acta Neuropathol Commun* **11**, 127 (2023).

24. Gomez-Arboledas A*, et al.* Phagocytic clearance of presynaptic dystrophies by reactive astrocytes in Alzheimer's disease. *Glia* **66**, 637-653 (2018).

25. Jiwaji Z*, et al.* Reactive astrocytes acquire neuroprotective as well as deleterious signatures in response to Tau and Ass pathology. *Nat Commun* **13**, 135 (2022).

26. Kim H*, et al.* Reactive astrocytes transduce inflammation in a blood-brain barrier model through a TNF-STAT3 signaling axis and secretion of alpha 1-antichymotrypsin. *Nat Commun* **13**, 6581 (2022).

27. Lines J*, et al.* Astrocyte-neuronal network interplay is disrupted in Alzheimer's disease mice. *Glia* **70**, 368-378 (2022).

28. Moonen S*, et al.* Pyroptosis in Alzheimer's disease: cell type-specific activation in microglia, astrocytes and neurons. *Acta Neuropathol* **145**, 175-195 (2023).

29. Patani R, Hardingham GE, Liddelow SA. Functional roles of reactive astrocytes in neuroinflammation and neurodegeneration. *Nat Rev Neurol* **19**, 395-409 (2023).

30. Nussbaum JM*, et al.* Prion-like behaviour and tau-dependent cytotoxicity of pyroglutamylated amyloid-beta. *Nature* **485**, 651-655 (2012).

31. Condello C, Yuan P, Schain A, Grutzendler J. Microglia constitute a barrier that prevents neurotoxic protofibrillar Abeta42 hotspots around plaques. *Nat Commun* **6**, 6176 (2015).

32. Baik SH, Kang S, Son SM, Mook-Jung I. Microglia contributes to plaque growth by cell death due to uptake of amyloid beta in the brain of Alzheimer's disease mouse model. *Glia* **64**, 2274-2290 (2016).

33. Zhou J, Singh N, Galske J, Hudobenko J, Hu X, Yan R. BACE1 regulates expression of Clusterin in astrocytes for enhancing clearance of beta-amyloid peptides. *Mol Neurodegener* **18**, 31 (2023).

34. Petrova E, Lopez-Gay JM, Rhiner C, Moreno E. Flower-deficient mice have reduced susceptibility to skin papilloma formation. *Dis Model Mech* **5**, 553-561 (2012).

35. Liu L*, et al.* Mitochondrial outer-membrane protein FUNDC1 mediates hypoxia-induced mitophagy in mammalian cells. *Nat Cell Biol* **14**, 177-185 (2012).

36. Cheng J*, et al.* Autophagy regulates MAVS signaling activation in a phosphorylation-dependent manner in microglia. *Cell Death Differ* **24**, 276-287 (2017).

37. Sandberg A*, et al.* Stabilization of neurotoxic Alzheimer amyloid-beta oligomers by protein engineering. *Proc Natl Acad Sci U S A* **107**, 15595-15600 (2010).

38. Sollvander S*, et al.* Accumulation of amyloid-beta by astrocytes result in enlarged endosomes and microvesicle-induced apoptosis of neurons. *Mol Neurodegener* **11**, 38 (2016).

39. Levayer R, Dupont C, Moreno E. Tissue Crowding Induces Caspase-Dependent Competition for Space. *Curr Biol* **26**, 670-677 (2016).

40. Moreno E, Fernandez-Marrero Y, Meyer P, Rhiner C. Brain regeneration in Drosophila involves comparison of neuronal fitness. *Curr Biol* **25**, 955-963 (2015).

41. Parker TM*, et al.* Cell competition in intratumoral and tumor microenvironment interactions. *EMBO J* **40**, e107271 (2021).

42. Vousden KH, Prives C. Blinded by the Light: The Growing Complexity of p53. *Cell* **137**, 413-431 (2009).

43. Maddika S*, et al.* Cell survival, cell death and cell cycle pathways are interconnected: implications for cancer therapy. *Drug Resist Updat* **10**, 13-29 (2007).

44. Xie JM*, et al.* TIGAR has a dual role in cancer cell survival through regulating apoptosis and autophagy. *Cancer Res* **74**, 5127-5138 (2014).

45. Kannan S*, et al.* Notch activation inhibits AML growth and survival: a potential therapeutic approach. *J Exp Med* **210**, 321-337 (2013).

46. Delbridge AR, Grabow S, Strasser A, Vaux DL. Thirty years of BCL-2: translating cell death discoveries into novel cancer therapies. *Nat Rev Cancer* **16**, 99-109 (2016).

47. Rudd JC*, et al.* Flower dependent trafficking of lamellar bodies facilitates maturation of the epidermal barrier. *Nat Commun* **16**, 6892 (2025).

48. Kalkavan H, Green DR. MOMP, cell suicide as a BCL-2 family business. *Cell Death Differ* **25**, 46-55 (2018).

49. Chipuk JE, Green DR. How do BCL-2 proteins induce mitochondrial outer membrane permeabilization? *Trends Cell Biol* **18**, 157-164 (2008).

50. Merrifield RB. Solid Phase Peptide Synthesis. I. The Synthesis of a Tetrapeptide. *Journal of the American Chemical Society* **85**, 2149-2154 (1963).

Acknowledgement

This work was supported by grants from the Deutsche Forschungsgemeinschaft (DFG), collaborative research center SFB894 (project number 157660137), subproject A10 (to H.-F.C. and E.K.), and A14 (to V.F.) and the University of Saarland (HOMFORexzellent 2020, NanoBioMed Young Investigator Grant 2020, and Anschubfinanzierung 2025 to H.-F.C.). We thank Keerthana Ravichandran, Margarete Klose, Anja Bergsträßer, Nicole Rothgerber, Katrin Sandmeier, Andrea Schottek and Christine Wesely for their excellent technical assistance.

Author contributions

H.-F.C. conceived and supervised the study. S.-M.T. performed all cellular fitness assays, molecular biology experiments, and tissue staining analyses. C.-H.L. and Y.S. assisted with neuronal culture preparation. L.Y. carried out AD human brain tissue sectioning and staining. J.H. performed laser microdissection of brain tissue. M.J. synthesized the peptides. A.C. and S.R. carried out the SPR analysis. W.J.S.-S. provided postmortem AD brain tissue. V.F. generated the Flower antibodies and Flower-gene-deficient mice. E.K. and H.-F.C. secured funding for the project. C.-K.Y. contributed essential intellectual input to the study. C.-K.Y., L.Y., E.K., and C.S. critically reviewed the manuscript. H.-F.C. wrote the manuscript with input from all authors. All authors reviewed and approved the final version of the manuscript.

Data availability

All data supporting the findings of this study are available within the paper and its Supplementary Information. Additional data are available from the corresponding author upon reasonable request. Source data are provided with this paper.

Competing interests

The authors declare no competing interests.

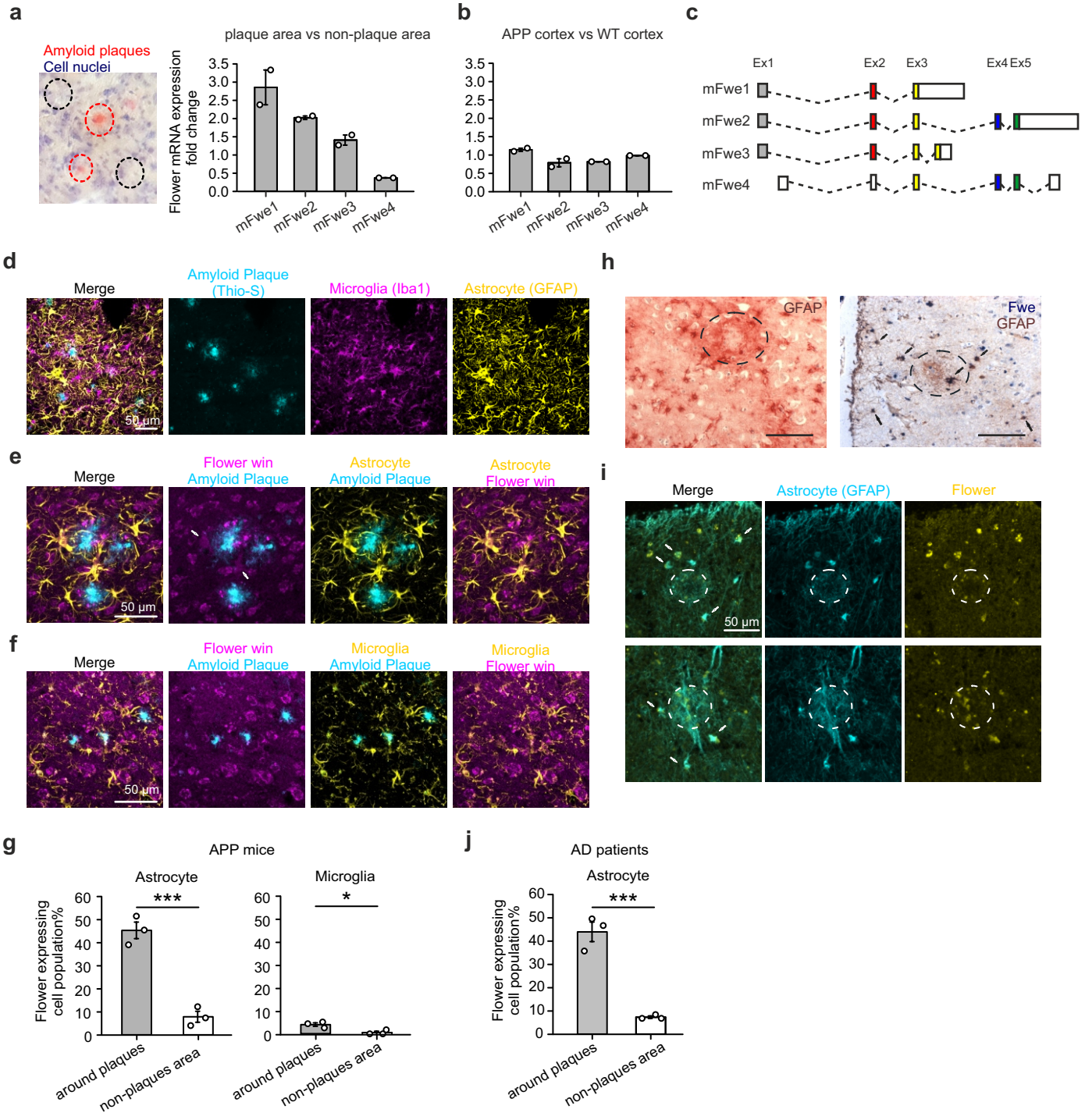
a
Amyloid plaques
Cell nuclei
plaque area vs non-plaque area
Flower mRNA expression fold change
mFwe1
mFwe2
mFwe3
mFwe4
b
APP cortex vs WT cortex
c
Ex1
Ex2
Ex3
Ex4 Ex5
d
Merge
Amyloid Plaque (Thio-S)
Microglia (Iba1)
Astrocyte (GFAP)
50 µm
e
Flower win Amyloid Plaque
Astrocyte Amyloid Plaque
Astrocyte Flower win
f
Microglia Amyloid Plaque
Microglia Flower win
h
GFAP
Fwe GFAP
i
Astrocyte (GFAP)
Flower
g
APP mice
Astrocyte
Microglia
Flower expressing cell population%
around plaques
non-plaques area
j
AD patients

Figure 1

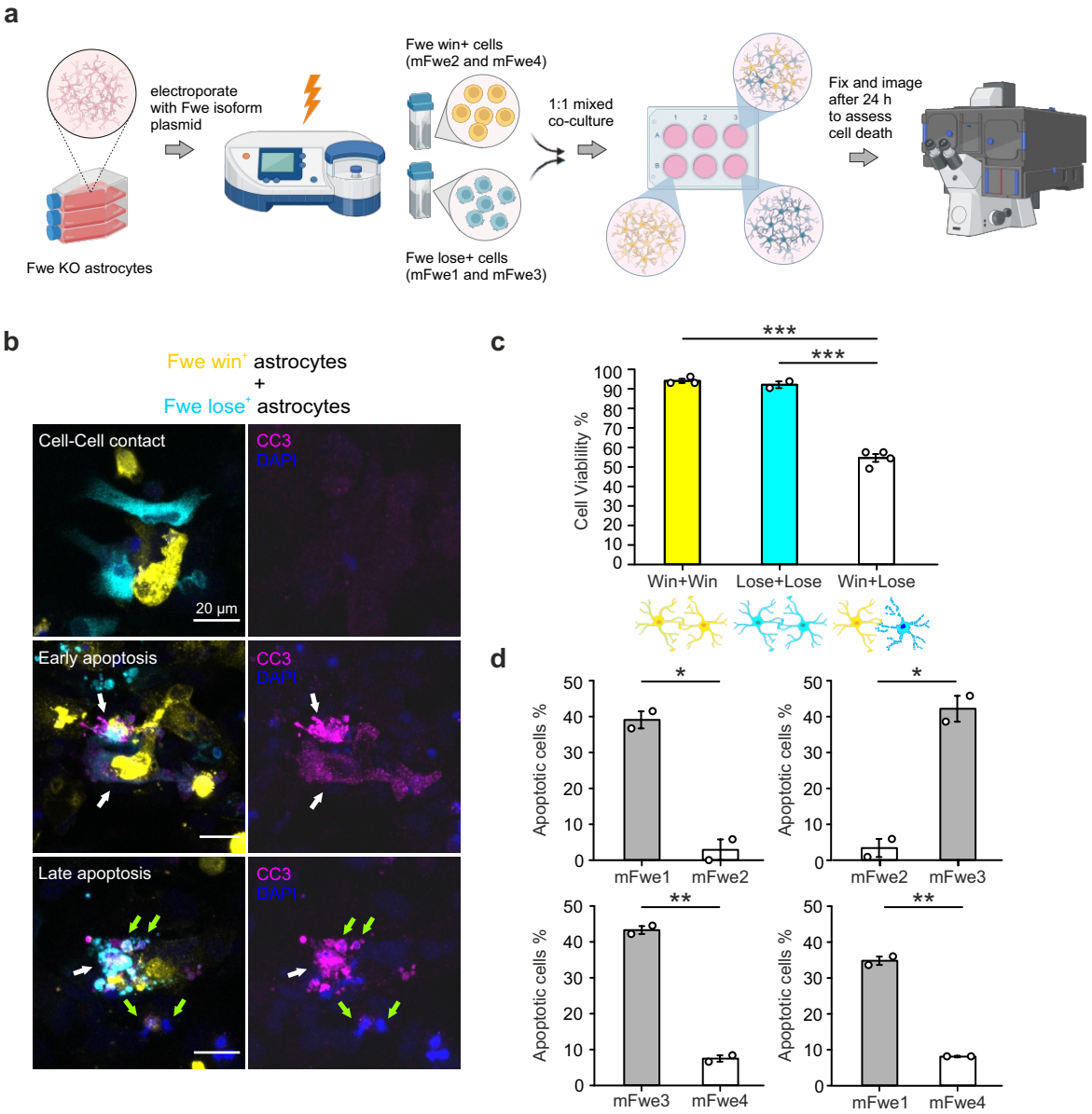
a
Fwe KO astrocytes
electroporate
with Fwe isoform
plasmid
Fwe win+ cells
(mFwe2 and mFwe4)
Fwe lose+ cells
(mFwe1 and mFwe3)
1:1 mixed
co-culture
Fix and image
after 24 h
to assess
cell death
b
Fwe win+ astrocytes
+
Fwe lose+ astrocytes
Cell-Cell contact
CC3
DAPI
20 µm
Early apoptosis
Late apoptosis
c
Cell Viability %
Win+Win
Lose+Lose
Win+Lose
d
Apoptotic cells %
mFwe1
mFwe2
mFwe3
mFwe4

Figure 2

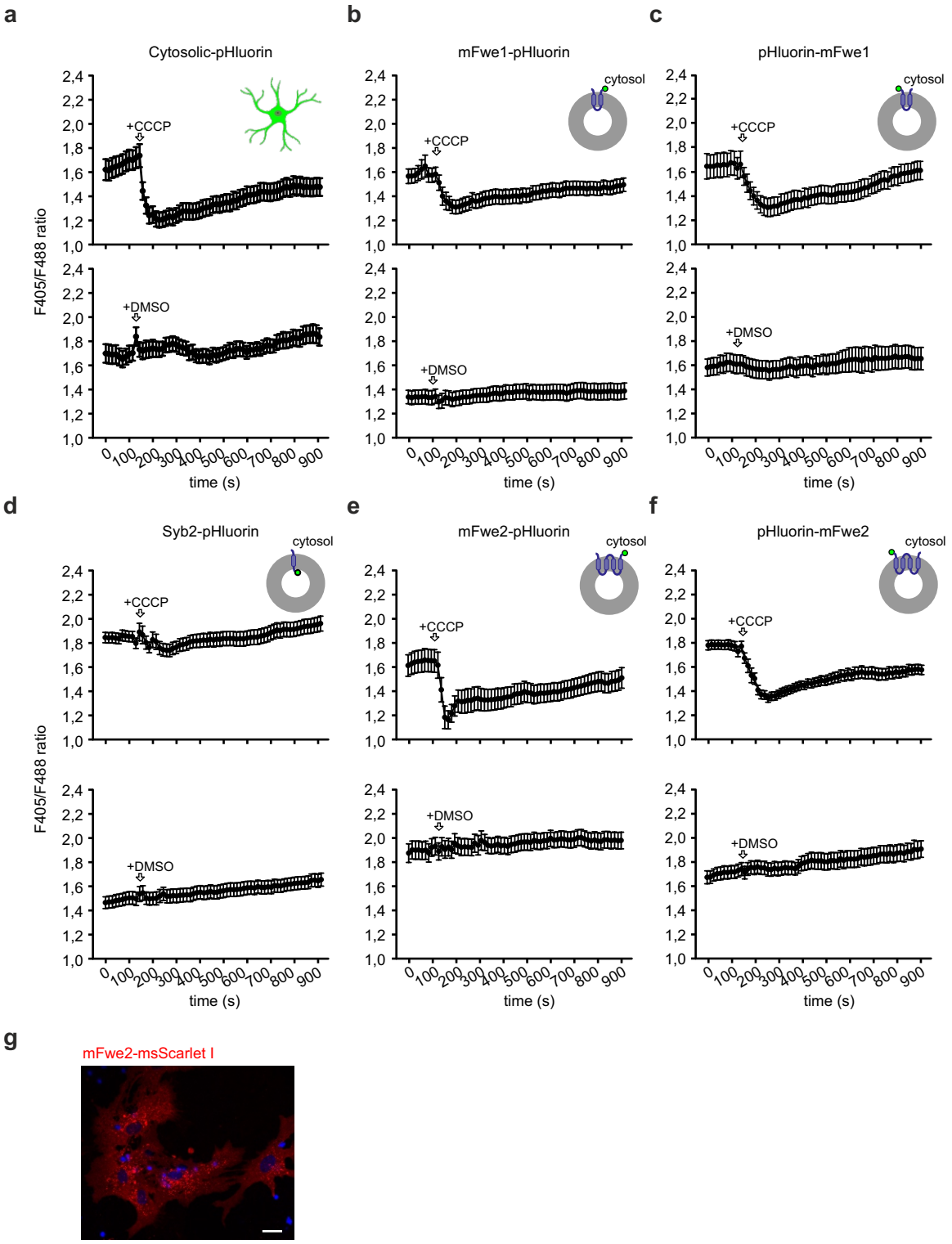
a
b
c
d
e
f
g
Cytosolic-pHluorin
mFwe1-pHluorin
pHluorin-mFwe1
Syb2-pHluorin
mFwe2-pHluorin
pHluorin-mFwe2
cytosol
+CCCP
+DMSO
F405/F488 ratio
time (s)
mFwe2-msScarlet I

Figure 3

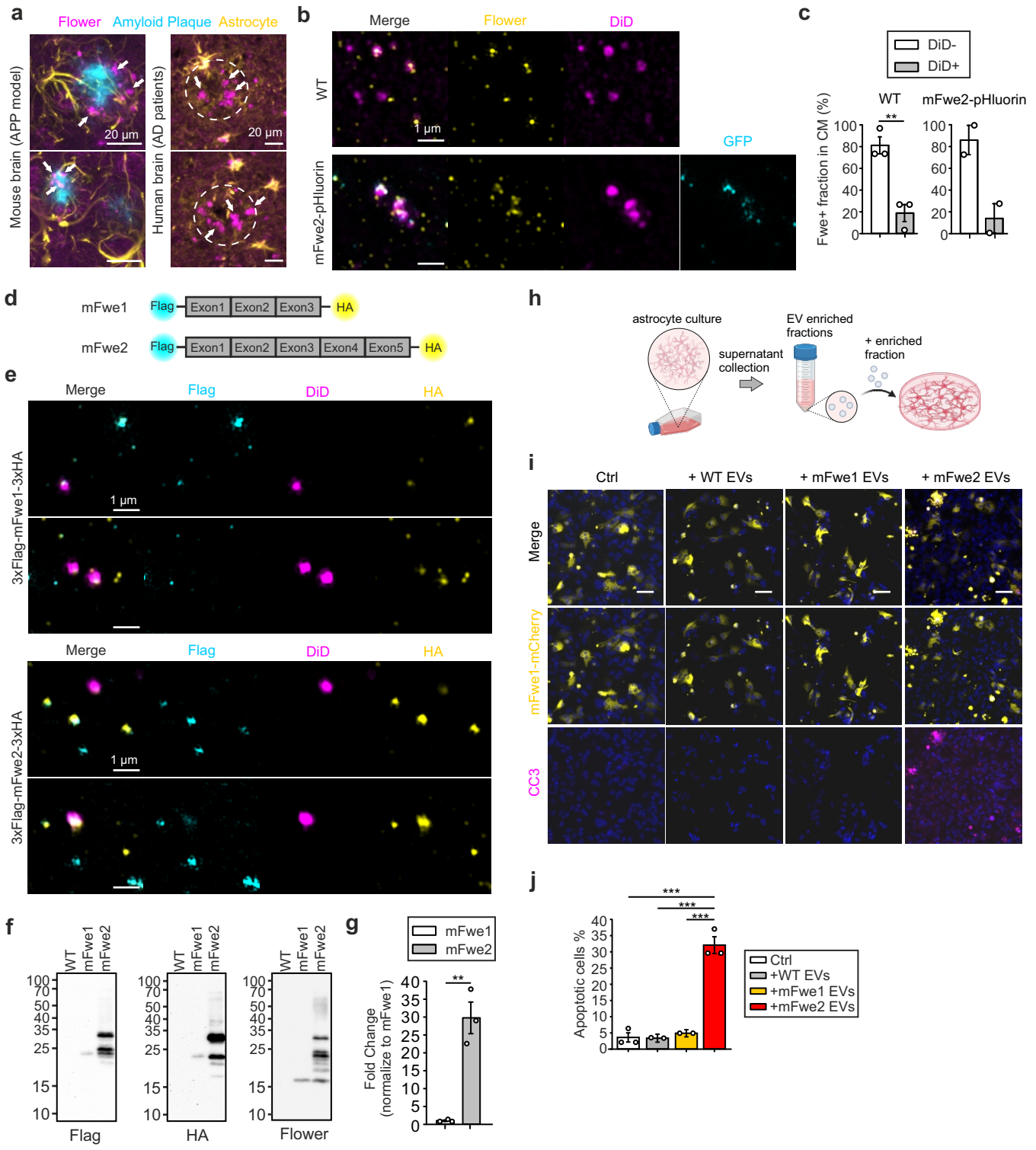
a
Flower
Amyloid Plaque
Astrocyte
Mouse brain (APP model)
Human brain (AD patients)
20 μm
b
Merge
Flower
DiD
WT
mFwe2-pHluorin
1 μm
GFP
c
DiD-
DiD+
WT
mFwe2-pHluorin
Fwe+ fraction in CM (%)
d
mFwe1
mFwe2
Flag
Exon1
Exon2
Exon3
Exon4
Exon5
HA
e
Merge
Flag
DiD
HA
3xFlag-mFwe1-3xHA
3xFlag-mFwe2-3xHA
1 μm
f
WT
mFwe1
mFwe2
Flag
HA
Flower
g
mFwe1
mFwe2
Fold Change (normalize to mFwe1)
h
astrocyte culture
supernatant collection
EV enriched fractions
+ enriched fraction
i
Ctrl
+ WT EVs
+ mFwe1 EVs
+ mFwe2 EVs
Merge
mFwe1-mCherry
CC3
j
Apoptotic cells %
Ctrl
+WT EVs
+mFwe1 EVs
+mFwe2 EVs

Figure 4

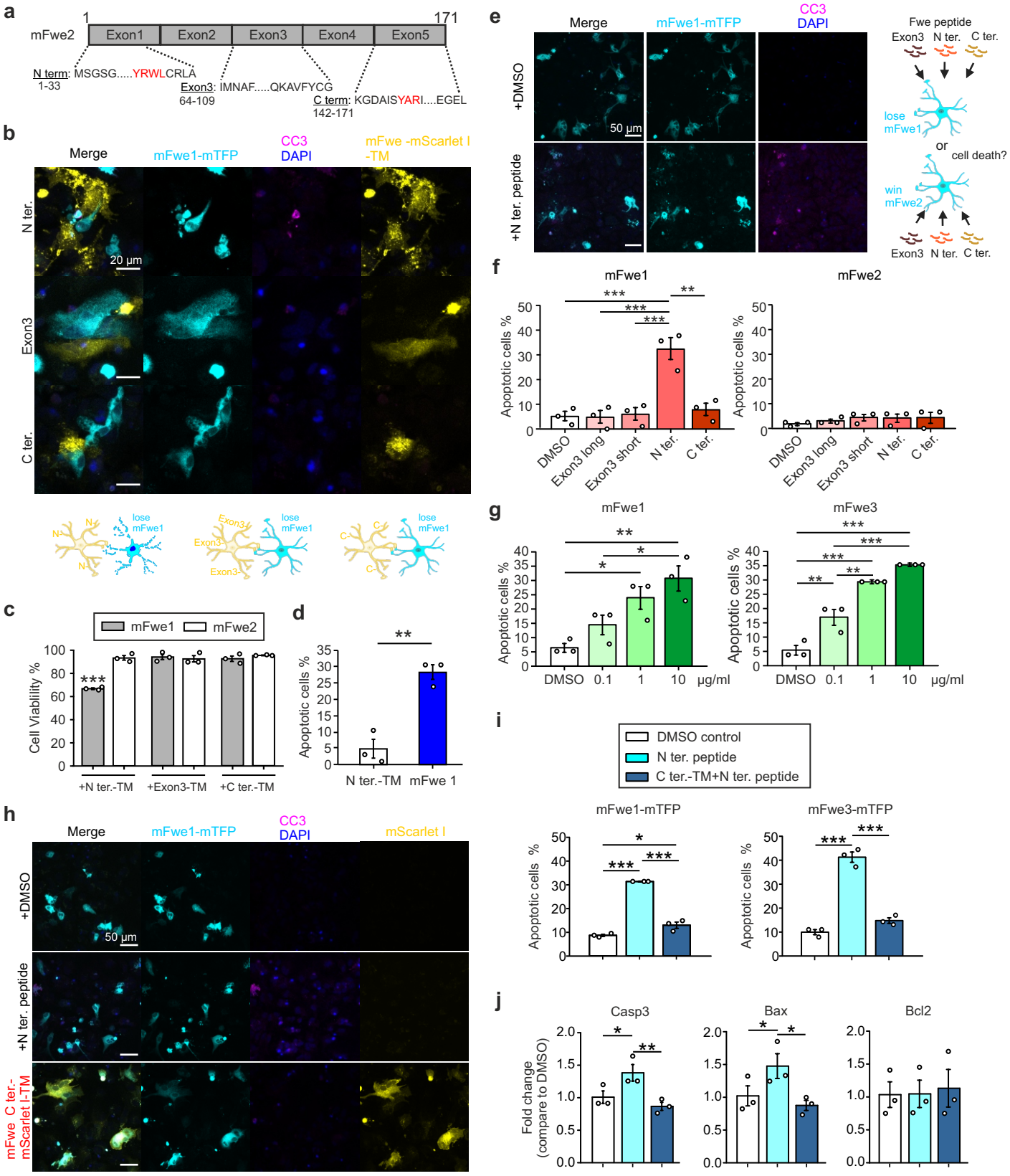
a
mFwe2
1
171
Exon1
Exon2
Exon3
Exon4
Exon5
N term: MSGSG.....YRWLCRLA
1-33
Exon3: IMNAF.....QKAVFYCG
64-109
C term: KGDAISYARI....EGEL
142-171
b
Merge
mFwe1-mTFP
CC3
DAPI
mFwe -mScarlet I -TM
N ter.
Exon3
C ter.
20 µm
lose mFwe1
c
mFwe1
mFwe2
Cell Viability %
+N ter.-TM
+Exon3-TM
+C ter.-TM
d
Apoptotic cells %
N ter.-TM
mFwe 1
e
Merge
mFwe1-mTFP
CC3
DAPI
+DMSO
+N ter. peptide
50 µm
Fwe peptide
Exon3
N ter.
C ter.
lose mFwe1
or
cell death?
win mFwe2
f
mFwe1
mFwe2
Apoptotic cells %
DMSO
Exon3 long
Exon3 short
N ter.
C ter.
g
mFwe1
mFwe3
Apoptotic cells %
DMSO
0.1
1
10
µg/ml
i
DMSO control
N ter. peptide
C ter.-TM+N ter. peptide
mFwe1-mTFP
mFwe3-mTFP
Apoptotic cells %
j
Casp3
Bax
Bcl2
Fold change (compare to DMSO)

h
Merge
mFwe1-mTFP
CC3
DAPI
mScarlet I
+DMSO
+N ter. peptide
mFwe C ter.-mScarlet I-TM
50 µm

Figure 5

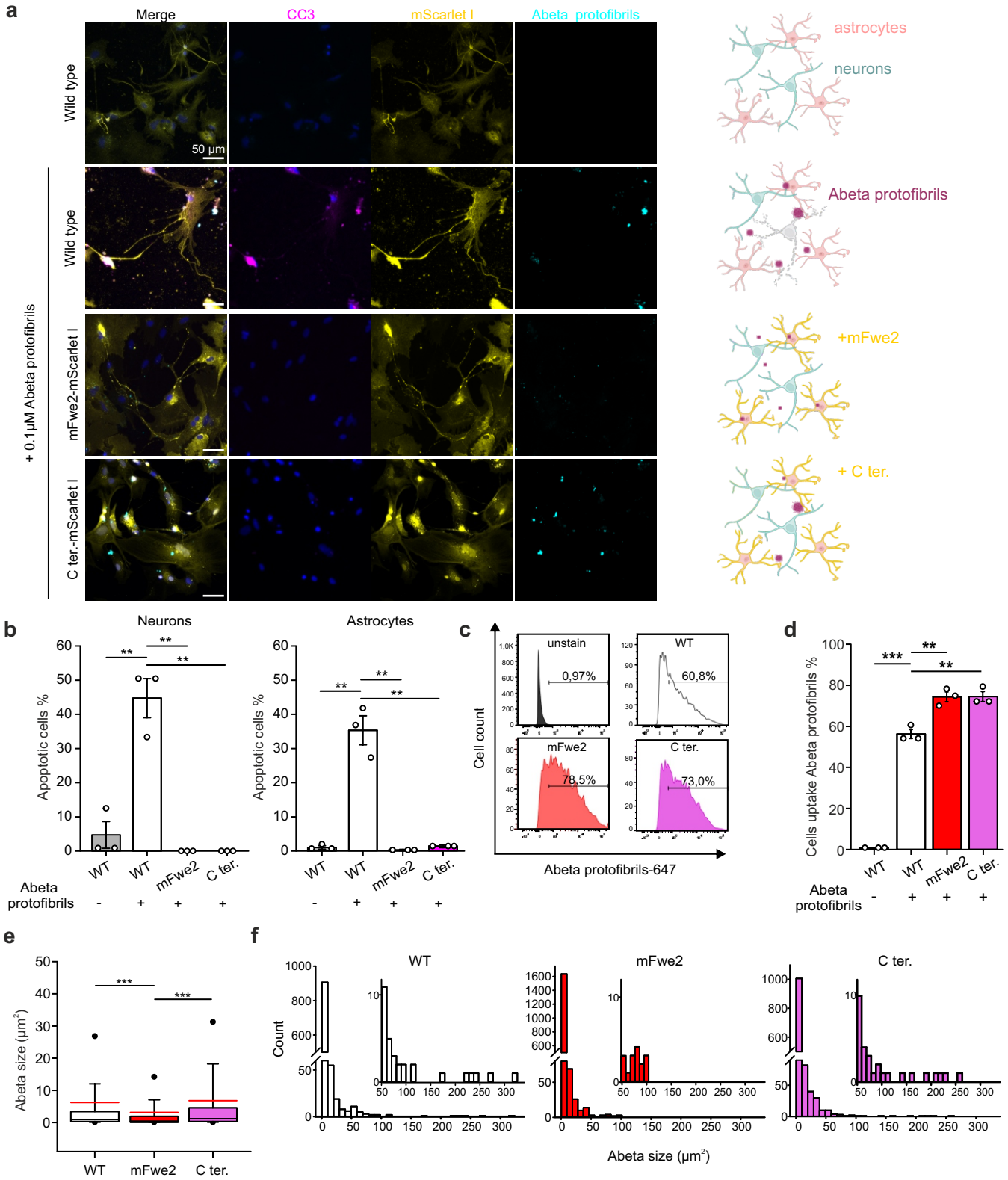
a
Merge
CC3
mScarlet I
Abeta protofibrils
Wild type
50 µm
Wild type
mFwe2-mScarlet I
C ter.-mScarlet I
+ 0.1µM Abeta protofibrils
astrocytes
neurons
Abeta protofibrils
+mFwe2
+ C ter.
b
Neurons
Astrocytes
Apoptotic cells %
WT
mFwe2
C ter.
Abeta protofibrils
c
unstain
0,97%
WT
60,8%
mFwe2
78,5%
C ter.
73,0%
Cell count
Abeta protofibrils-647
d
Cells uptake Abeta protofibrils %
e
Abeta size (µm²)
f
Count
Abeta size (µm²)

Figure 6

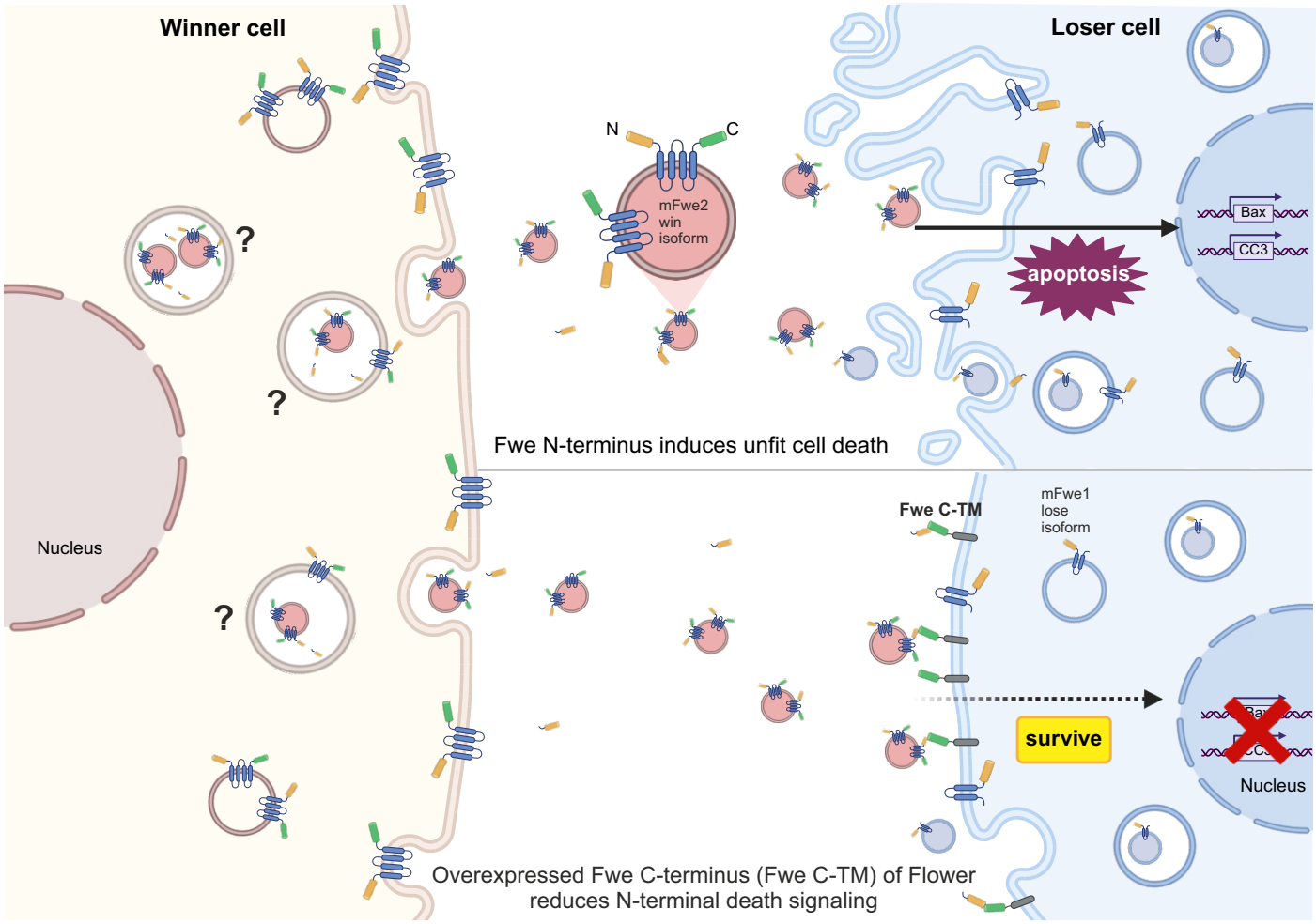
Winner cell
Loser cell
N
C
mFwe2
win
isoform
?
?
?
Nucleus
Bax
CC3
apoptosis
Fwe N-terminus induces unfit cell death
Fwe C-TM
mFwe1
lose
isoform
survive
Nucleus
Overexpressed Fwe C-terminus (Fwe C-TM) of Flower
reduces N-terminal death signaling

Figure 7

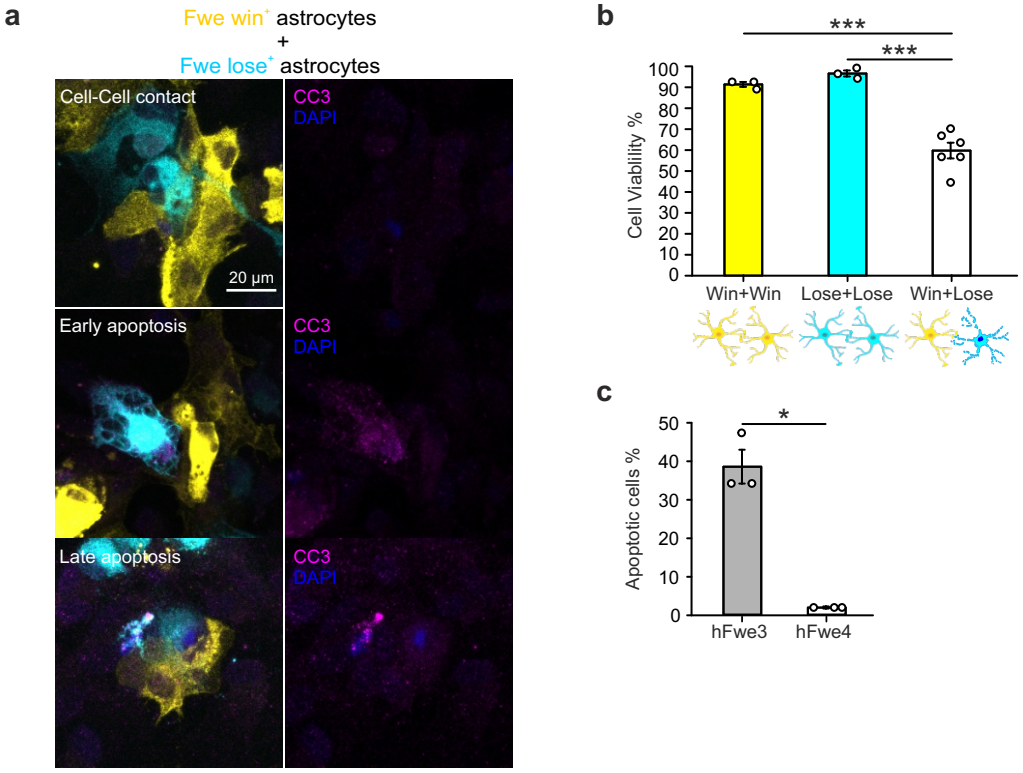

Extended Data Fig. 1

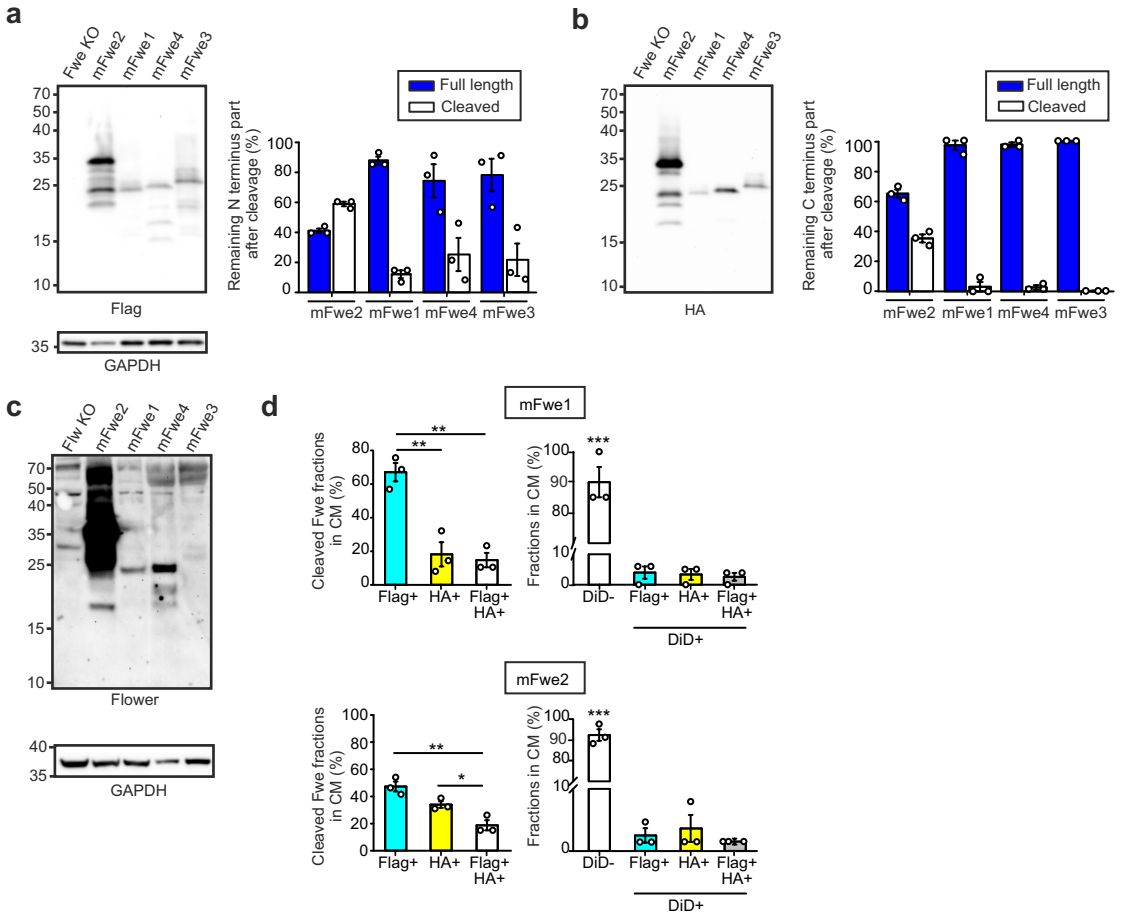

Extended Data Fig. 2

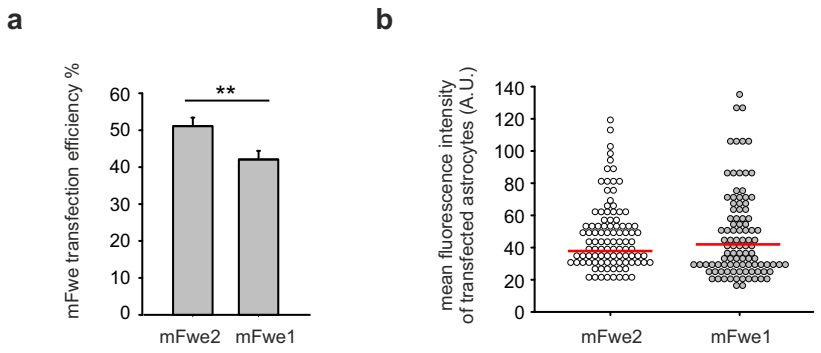

Extended Data Fig. 3

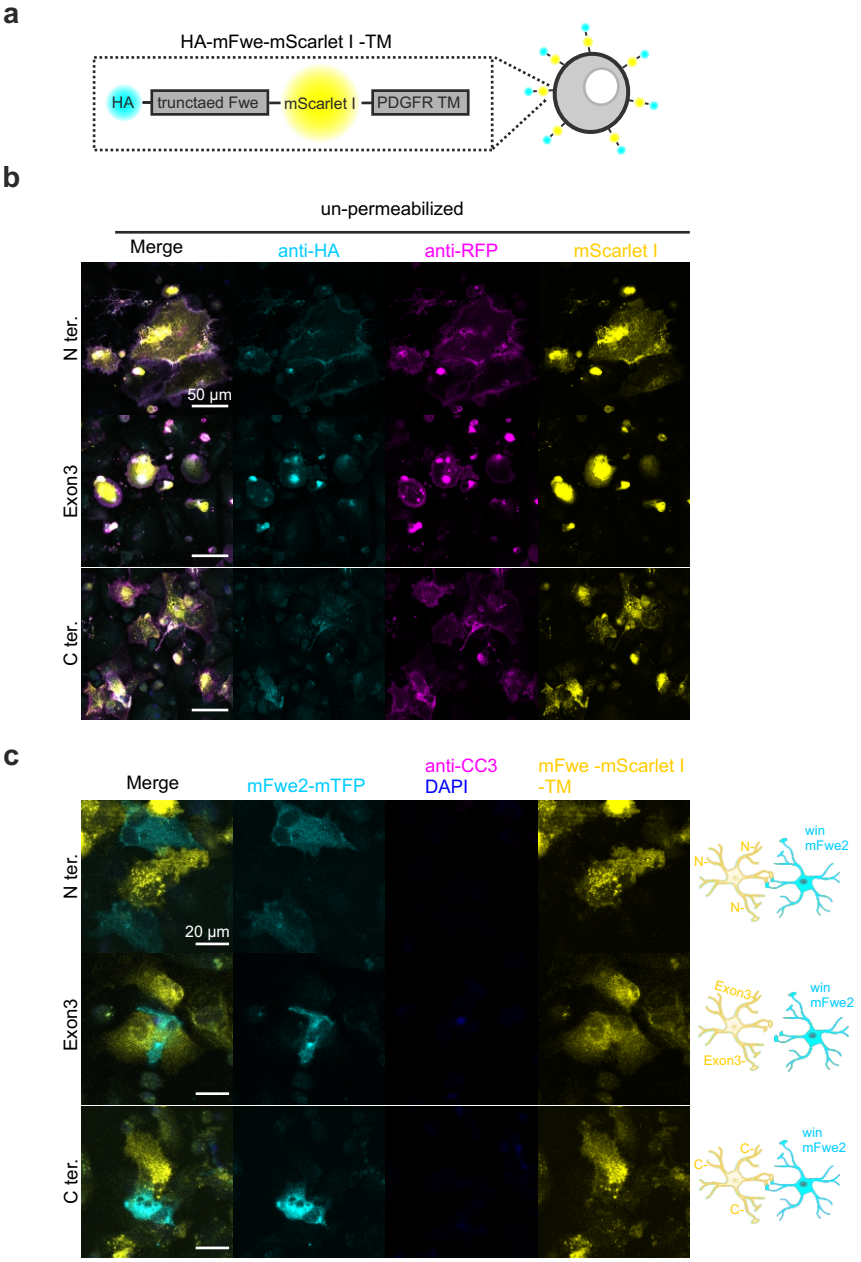

Extended Data Fig. 4

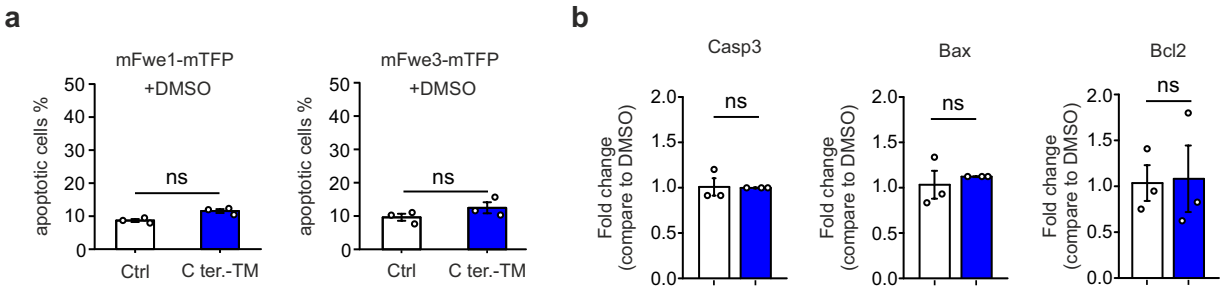

Extended Data Fig. 5

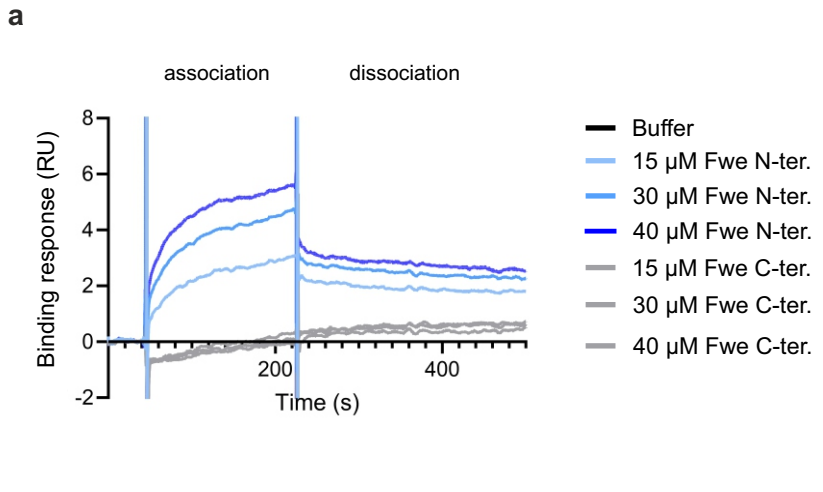

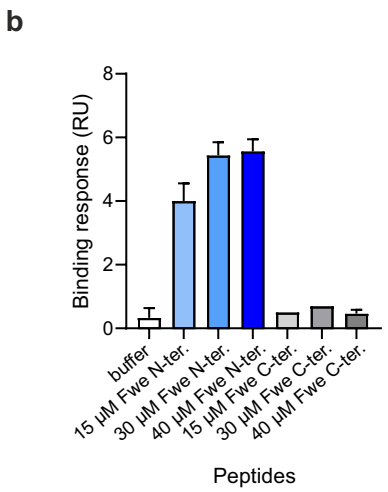

Extended Data Fig. 6